2009

A Parametric study of gas sensing response of ZnO nanostructures and carbon nanotubes

Amandeep S. Saluja

A Parametric Study of Gas Sensing Response of ZnO Nanostructures and Carbon Nanotubes

By

Amandeep S. Saluja

A Thesis Submitted

In Partial Fulfillment

Of the Requirements for the Degree of

Masters of Science

In

Microelectronic Engineering

Approved by:

Prof: _____
Dr. Seth M. Hubbard (Thesis Advisor)

Prof: _____
Dr. Lynn F. Fuller (Committee Member)

Prof: _____
Dr. Ryne P. Raffaelle (Committee Member)

Prof: _____
Dale Ewbank (Committee Member)

DEPARTMENT OF MICROELECTRONIC ENGINEERING

KATE GLEASON COLLEGE OF ENGINEERING

ROCHESTER INSTITUTE OF TECHNOLOGY

ROCHESTER, NEW YORK

July, 2009

A Parametric Study of Gas Sensing Response of ZnO Nanostructures and Carbon Nanotubes

By

Amandeep S. Saluja

_____ _____

Amandeep S Saluja July, 2009

Dedicated to my wife
For her continued love and support.

ACKNOWLEDGEMENTS

I would like to thank Dr. Seth Hubbard for his support and guidance during the course of this project. I greatly appreciate all the time and effort he spent to get me up to speed and his guidance during the advancement of the project. In addition, I would like to thank the members of the committee Dr. Ryne Raffaelle, Dr. Lynn Fuller and Prof. Dale Ewbank for their guidance and their time in reviewing my thesis. I would also like to thank Dr. Lei Kerr, Dr. Brian Landi, Chris Schauerman, Roberta DeLio and Annick Anctil for providing the raw materials I needed for the project and many useful discussions without which this project would not have been possible. I would like to take this opportunity to extend my regards to all the staff members of SMFL for their continued support and enthusiasm during the course of the project. This work would not have been possible without their help. I would also like to thank Dr. Cory Cress for all his help with several conceptual discussions pertaining to intricate details of the project. I would also like to thank soon to be Drs, Chris Bailey and Ivan Puchades for all their help with the fabrication processes and other phases of the research. I would also like to thank my fellow graduate students and colleagues Sankha Mukherjee, Rob Manley, Sunwoo Lee, Keerti Kalia and Binoy Chedda for all their help and support. Finally, I would like to thank my family for their continued love and support. I am especially grateful to my wife Harshita Shastri and my parents Mr. Manmohan Singh Saluja and Mrs. Swaranjeet Kaur Saluja for helping me keep focused and for always supporting me in achieving my dreams.

TABLE OF CONTENTS

LIST OF TABLES

LIST OF FIGURES

Abstract

Solid state chemical sensors are gaining popularity and finding extensive use in process control, environmental monitoring and residential safety. ZnO, a semiconducting metal oxide, and carbon nanotubes (CNTs) have attracted great interest over the years for their sensitivity to a variety of gases. Nanostructured sensing materials, such as nanowires, nanotubes and quantum dots offer an inherently high surface area, thus reducing operating temperatures and increasing sensitivity to low concentrations of analytes. In this work, ZnO nano-structures and CNTs have been tested as chemical sensors and a detailed study on the effect of different process parameters such as temperature, carrier gas flow, inter-electrode spacing, gas concentration and material properties on gas sensitivity is presented.

Initial ZnO nanoparticles were prepared by a simple solution chemical process and characterized by Secondary Electron Microscopy (SEM) and Brunauer, Emmet and Teller (BET) Sorptometer to demonstrate the morphology and surface area respectively. The gas sensor platforms consisted of Pt inter-digitated fingers with a spacing of 10 μm. The sensor platform was dip-coated with ZnO nano-platelets suspended in terpineol to form a uniform film. Sensing was performed in a closed quartz chamber where, high purity N_2 and dry industrial air were used as carrier and recovery gas respectively. Sensitivity of nano-platelets and porous films was measured for different concentrations of the analyte (H_2). High response was observed at room temperature for H_2 gas with sensitivities in excess 80% for 60ppm and about 55% for 80ppm of H_2 gas at room temperature was observed for the nano-platelets and the porous films respectively. High sensitivity of the sensor at low temperatures is attributed to both the increased surface

area of the porous ZnO nano-platelets and the presence of a Pt catalyst. Measurements at higher temperatures (150 °C) show even higher sensitivities, near 96% for a 20 ppm H_2 concentration. Sensitivity with different gases and organic solvents was also measured at operating temperatures of 200°C. Values on the order of 60%, 42% and 29% for 315 PPM of CO, O_2 and NH_3 whereas sensitivity values of 77.76%, 70.26% and 38.43% for C_2H_5OH, CH_3OH and H_2O were recorded for concentration values approximating 500 PPM. The sensors depict incomplete recovery of resistance at room temperature. This effect is possibly due to the traces of elemental Zn in the material, which were not oxidized at the time of recovery. However, this effect was not observed at higher temperatures.

Designed experiments conducted to understand effects of various device and process parameters show negative dependence of spacing on sensitivity with maximum effect of applied bias for lower concentration values. The sensitivity of the sensor was also recorded to increase with the increase in the number of electrodes. Higher sensitivity values nearing 70% were achieved with 30 IDEs for 60 PPM H_2 when compared to 60% for 60 PPM of H_2 with 20 IDEs. Interaction effects were observed and implemented to understand and model the behavior of the gas sensor.

Sensitivity of arc produced CNTs was measured to various gases and organic solvents. Values on the order of 24% were observed at 80 PPM CO as compared to values of sensitivity about 15% for O_2 and 3% for H_2. Also, sensitivity value of 15% was measured for as low as 4 PPM of DMA which suggests the capability of PPB levels of DMA using CNTs. A brief comparison of sensitivity values achieved for ZnO nano-platelets and CNTs with similar analytes was also presented.

Sensitivity to different analytes was measured using impedance spectroscopy for HiPCo produced SWCNT network. For experiments conducted with varying exposure time, sensitivity values nearing 6% for 0.01% (100 PPM) DMA for an exposure time of 25 minutes were recorded. Sensitivity values recorded for other solvents were 16.74%, 10.98%, 7.97%, 6.96% and 4.28% for concentration levels of 2.04%, 4.02%, 2.04%, 14% and 6.05% of NH_3, IPA, CO, CH_3OH and C_2H_5OH respectively. For experiments with varying concentration values of different analytes, higher response was observed for gaseous analytes. Results on the order of 15.27% and 3.82% were recorded for as low as 0.18% of both NH_3 and CO. For the organic solvents, values approximating 2.64%, 2.36% and 0.10% for concentration levels of 0.29%, 0.92% and 0.42% of IPA, CH_3OH and C_2H_5OH respectively. Results obtained with HiPCo produced SWCNT network at room temperature were comparable to the values of sensitivity shown by other researchers.

Our future works entails correlating the sensitivity of the gas sensors to the material properties in addition to the device and the process parameters, with further development in methods for fabricating gas sensors and improvement in the selectivity of the sensor. For CNT based sensors, using as-grown multiwall carbon-nanotubes MWCNTs for gas sensor fabrication would be the next step in this research. In addition to developing standard fabrication techniques, further research is required for improving selectivity for different gases and organic solvents by decorating or filling CNTs with metal nano-particles or different groups of organic molecules. Also, future work will be focused to correlate sensitivity of HiPCo produced SWCNTs, Laser ablated SWCNTs and MWCNTs to their material properties.

CHAPTER I

INTRODUCTION

1.1 The importance of Gas Sensors

For many years, gas sensors have attracted great deal of interest for their potential use in various fields such as process control, environmental monitoring and residential safety [1]. Some of these include air quality monitoring, smoke alarms, mine and tunnel warning systems, greenhouses, breath analyzers, dangerous LPG leak in cars or in service stations and storage tank environment.

With the advancement in technology, the need for precise and sensitive gas sensors continues to increase. Over the last few decades, researchers around the world have been able to meet this demand with the use of advanced technology and novel materials. In this context, solid state chemical sensors have been gaining popularity and finding extensive use for their higher sensitivity and smaller size. Also, with the advent of Nanotechnology, scientists have been able to achieve new horizons in the field of gas sensors.

Nanotechnology can be defined as the engineering of functional systems at nanoscale. At this scale, properties exhibited by the materials are not similar to the properties at the macro scale. Gas sensors constructed at the nanoscale are extremely sensitive, selective, and responsive and thus, the impact of nanotechnology on gas sensors is huge [1,2].

Nanostructured semiconducting metal oxides and other nanostructured sensing materials such as carbon nanotubes (CNTs) have been the main materials of interest for their attractive properties and versatile use. These nano-materials offer an inherently high surface to volume ratio, thus increasing the available surface area and yielding highly sensitive gas sensors with the ability to detect very low concentration of analytes [2,3]. In addition, these nanostructures help in lowering the operating temperature of the reaction. This reduction in operating temperatures by the use of novel nanostructured materials leads to low power consumption, thus allowing use of micromachined gas sensors and integration with other integrated circuits.

1.2 Material Properties of ZnO nano-structures and CNTs

ZnO, a semiconducting metal oxide, has attracted great interest over the years for its possible use in wide range of applications such as sensors, solar cell electrodes [4,5], optical waveguide device [6], and light emitting device [7]. Gas sensing properties of various ZnO nano-structures and ZnO based thin films have been widely investigated for their sensitivity to a variety of analytes [8,9,10]. In the past, many researchers have reported high operating temperatures ($200^{o}C$–$500^{o}C$) for ZnO based gas sensors [11,12]. These high operating temperatures have limited the use of semiconducting metal-oxides in micromachined gas sensors for their high power consumption. However, with the recent developments in the field, researchers have reported much lower operative temperatures for metal-oxide based gas sensors.

ZnO nanostructures can be prepared using simple techniques such as dissolving ZnO particles or chemical bath depositions [13]. Various morphologies for these synthesized nanostructures have been demonstrated by varying the process conditions. Depending on the shape and size of the synthesized nanostructure, the material can exhibit different electrical properties in terms of having a very high or low resistance. Also, the variation in the mechanical properties of the material makes it attractive to be used in other novel applications such as MEMS based pressure sensors [14]. These versatile properties and simple synthesis techniques for ZnO has resulted in its use for various applications and novel gas sensors.

Chemisorption of the analyte on the surface of the sensing film is the primary sensing mechanism for the ZnO based gas sensors presented in this study. However, the resistance encountered in collecting the charge delivered during the sensing phase results in a slow response of the sensor when compared to other novel materials like CNTs.

CNTs have been proven to be a promising material for a number of commercial and scientific applications like flat panel displays, novel semiconducting devices, hydrogen storage devices, chemical and electromechanical sensors [15]. Modern CNT based gas-sensor devices are reported to operate at room temperatures with abilities to detect analytes in the parts per billion (PPB) level [16]. Additionally, CNTs can be functionalized (using different polymers/functional groups) or decorated (using metal nanoparticles) to improve their sensitivity and selectivity to different gases and organic solvents. These properties make CNTs a preferred choice for novel gas sensor devices.

CNTs are created by rolling up a hexagonal lattice of graphite. Rolling the lattice at different angles creates a visible twist in the CNTs molecular structure, though the

overall shape remains cylindrical. This twist is called chirality. Based on the rolling angle, three types of nanotubes are possible: armchair, zigzag, or chiral. A thirty degree roll produces an armchair pattern and a zero degree roll makes a zigzag. Any intermediate angle produces a chiral nanotube. The names 'armchair' and 'zigzag' refer to the pattern of carbon bonds around the tube's circumference. The CNTs chirality, along with its diameter, determines its electrical properties. The armchair structure has metallic characteristics. Both zigzag and chiral structures produce band gaps, making these nanotubes semiconductors [17]. This unique property of CNTs to behave semi-conducting or metallic based on the diameter and chirality's [18], has been under investigation for making novel gas sensors. Figure 1 shows models of different configurations of carbon nanotubes [17].

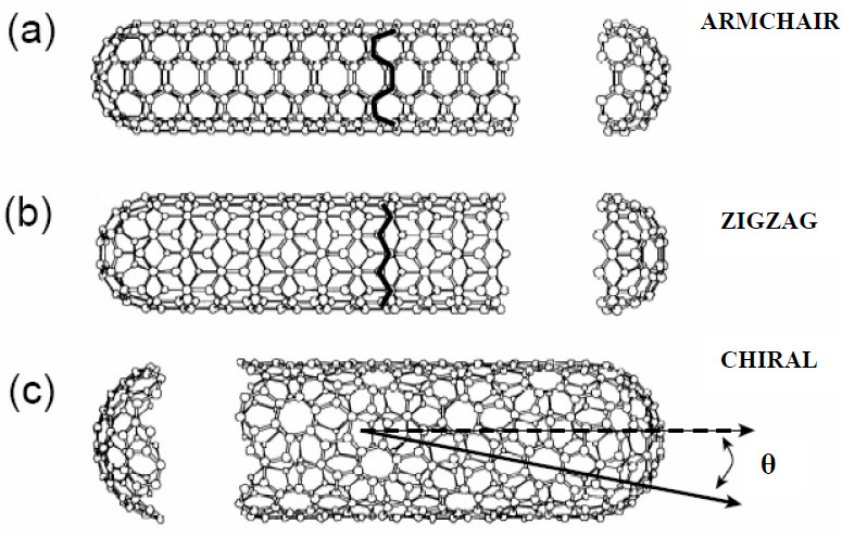

Fig 1: Models of armchair, zigzag and chiral carbon nanotubes

Factors affecting the choice of material for gas sensor fabrication are cost, availability, purity and sensitivity to different analytes. ZnO and other nanostructured

semiconducting metal oxides are cheap, easily available and easy to synthesize as a result, these materials have been used extensively over the years for gas sensor fabrication [1,2,3,8,9,10]. However recent discovery of CNTs and their sensitivity to different analytes, lower operating temperatures, faster response times and shorter recovery times has attracted great interest for their potential use in gas sensors [15,16,18], but synthesis of good quality CNTs by Laser Ablation or Chemical Vapor Deposition methods, involves sophisticated tools and is limited at this time. Also the quality of commercially available CNTs varies from different manufacturers and different methods of synthesis, which makes in-house characterization necessary in order to understand the sensitivity with respect to its material properties. Table 1 compares the two materials for different factors. As both ZnO and CNTs have some advantages and disadvantages, it is difficult to choose the material for fabrication of gas sensors unless the application is specified.

Factor	ZnO	CNTs
Cost	Low	High
Availability	Easily Available Commercially	Limited Suppliers
Synthesis	Easy (Chemical Bath Deposition)	Requires Sophisticated Tools
Purity	Good	In-house purification necessary.
Operating Temperatures	High (200°C-500°C)	Low (Room Temperature)
Sensitivity to different analytes	CO,NH_3,CH_4,H_2,NO_2,H_2S,DMA	O_2,NO_2,NH_3,H_2,H_2O,CO_2

Table 1: Comparison of ZnO and CNTs for different factors of comparison.

This project concentrates on fabricating highly sensitive gas sensors- using nanostructured ZnO and CNTs - operating at room temperature or slightly higher, and to

model the sensitivity of the gas sensors as a function of the input parameters. These parameters include process parameters such as temperature, concentration & carrier gas flow; material properties such as morphology & surface area and device parameters such as inter electrode spacing & number of electrodes. Initial efforts involved fabrication of gas sensors on commercially available platforms using ZnO and CNTs synthesized at Miami University of Ohio and Nanopower Research Labs respectively. Also gas sensor design and sensor platforms were optimized for these nano materials, using microelectromechanical systems (MEMS) technology. A brief study using the in-house fabricated -single level- MEMS gas sensors was conducted to understand the effect of different device parameters such inter electrode spacing and the number of electrodes on sensitivity of the sensors. Also a detailed study on the effect of temperature, carrier gas flow, gas concentration and material properties on gas sensitivity was conducted for hydrogen gas with ZnO based gas sensors.

1.3 Gas Sensor Background

Solid-state sensors are commercially available from several manufacturers and can detect a variety of gases [19]. However, researchers have been exploring different possibilities for lowering the operating temperatures and optimizing the sensor response in terms of sensitivity, selectivity, shorter response times and faster recovery times. Over the years researchers have developed and studied different types of gas sensors based on different working principles. These could be classified as:

1. Resistive Gas Sensors [20] - sensing film is deployed over inter-digitated electrodes (IDE) and the change in resistance of the film is monitored on exposure to the analyte –
2. Capacitive Gas Sensors [21] - use the sensing film as one of the terminals of the capacitor. On exposure to the analyte the adsorption of the analyte on the sensing film results in a change in capacitance, this change determines sensitivity to the analyte - ,
3. Optical Gas Sensors [22] - some materials undergo a change is absorbance on exposure to the analyte. This principle is used to monitor the change in absorption of the sensing film on exposure to the analyte - ,
4. FET based gas sensors [23] - sensing elements, usually CNTs, are used between two contacts and the change in voltage across the circuit is measured on exposure to gas. The change in electrochemical properties on CNTs on adsorbtion of the analyte forms the basis of FET based sensors.

The reaction at the surface of the adsorbent follows the basic steps in a heterogeneous reaction. This involves the diffusion of the reactants to the surface, promoting the adsorbtion of the analyte on the surface of the adsorbent. This adsorbtion is governed by Langmuir's theory of isotherms [24]. The reaction between the adsorbent and the adsorbate on the surface then causes the change in current of the system, which is recorded in order to obtain the sensitivity of a material to the analyte. The change is current depends on the number of reaction sites available for a given material system and will be discussed in detail in the subsequent sections. Once the available reaction sites are

occupied the sensing material can be recovered to its original state. This is due to the desorption of the analyte from the surface. The products formed at the surface then diffuse into the bulk thus returning the material back to its initial state. All the steps described above are stated below as per the order of their occurrence in the reaction [25].

1. Diffusion of the reactant(s) to the surface.
2. Adsorption of reactants to the surface.
3. Reaction on the surface of the sensing film. (Response Phase)
4. Desorption of the products from the surface (Recovery Phase)
5. Diffusion of the products into the bulk

ZnO based gas sensors have been the topic of research over the last few decades as they are easy to synthesize and easily available commercially. The sensing mechanism proposed in the literature involves reaction of the analyte with the sensing film at the surface [26]. This reaction can be either oxidizing or reducing in nature resulting in the change in concentration of electrons at the surface of the sensing film. This change is measured in terms of the net change in resistance which is used to define the sensitivity of the gas sensor given with the following equation [26].

$$S(\%) = \frac{R_{air} - R_{gas}}{R_{air}} * 100 \qquad \text{Eq [1]}$$

The reversible nature of this reaction enables the recovery of the material when the flow of the sensing gas is terminated. Usually an inert gas like N_2 or Argon is used as a carrier gas whereas air [23] is used as recovery gas for experiments carried out under controlled environments. However, when these sensors are packaged and deployed for

sensing gases in the field, interference from other gases are minimized by the use of filtering materials which absorb all other gases except the sensing gas. Sensitivity of ZnO to various gases and organic solvents such as Carbon-Monoxide (CO) [27], Ammonia (NH_3) [8], Methane (CH_4) [9], Hydrogen (H_2) [28], Nitrogen Dioxide (NO_2) [29], Hydrogen Sulphide (H_2S) [26], Ethanol (C_2H_5OH) [30] and Dimethylamine (DMA) [31] has been reported at operating temperatures in the range of 100°C – 600°C. Table 2 summarizes the results reported for the sensitivity of ZnO to different analytes.

Morphology	Analyte	Temperature	Lowest Concentration Detected	Response Time
ZnO nanowires	CO	320 °C	500 PPM	20-25 Seconds
ZnO Thin Films	NH_3	25 °C	500 PPM	2 Min
ZnO Thin Films	Methane	250 °C	.1 % Methane	16.3 Seconds
ZnO	H_2	550-600 °C	200 ppm	55 Seconds
ZnO Nano Particles	NO_2,H_2S	300 °C	1 PPM NO2, 12 PPM H2S	20 Min
ZnO Nano Wires	C_2H_5OH	300 °C	1 PPM	Instantaneous
ZnO Nano Particles	DMA	300 °C	1% DMA	4.2 Min

Table 2: Summary of the results reported for sensitivity of ZnO to different analytes.

Efforts to lower the operating temperatures led to the use of nano structured ZnO because of their high surface to volume ratio. Some of the commonly used forms of ZnO are nano-particles [28], nano-nails, nano-wires [10], nano-rods [32], tetrapods [33], nano-pillars [34], nano-belts [35] and ZnO thin Films [8] some of which are shown in the figures below.

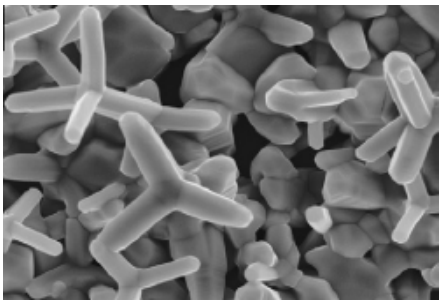

Fig. 2: ZnO Based Tetra-pods [33]

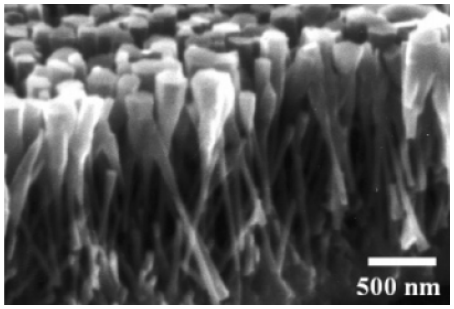

Fig. 3. ZnO Based Nano-Wires [10]

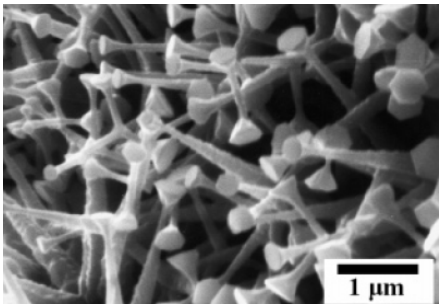

Fig. 4. ZnO Based Nano Nails [10]

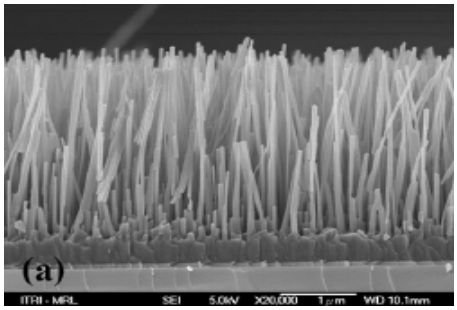

Fig. 5. ZnO Based Nano Wires [27]

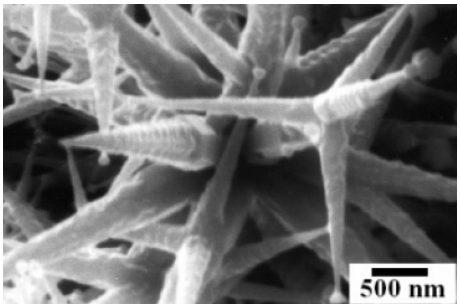

Fig. 6. ZnO Based Nano-Trees [10]

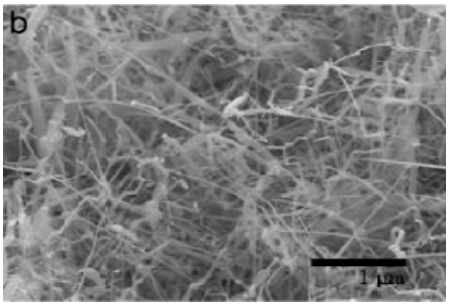

Fig. 7. ZnO Based Nano Belts [35]

Shorter response and recovery times at lower operating temperatures have been reported for porous nano-solids in the past [36]. This can be seen as in Table 3. The optimum operating temperature for the porous nanosolids was reported to be around 370^{o}C when compared to the conventional ZnO material with optimum operating temperature of about 430^{o}C. In addition to the foresaid, the use of a catalyst has been investigated to improve the sensitivity for gas sensors by Gong et al [37]. Significant

response for copper doped ZnO films was recorded for as low as 6 PPM CO at 150°C as compared to the negligible response observed for the undoped ZnO films at concentrations as high as 5000 PPM CO at 350°C.

Temperature	Sensors	Ethanol	Acetone	Benzene	Toluene	Xylene
370 °C	S-1	14 (19)	4 (9)	3 (5)	3 (4)	9 (3)
	S-2	8 (15)	3 (5)	2 (3)	2 (3)	7 (3)
420 °C	S-1	17 (6)	12 (7)	5 (6)	4 (5)	8 (4)
	S-2	3 (4)	2 (7)	2 (3)	2 (2)	2 (2)

Response time: from original value to 90% maximum changing value; recovering time: from 100 to 10% maximum changing value.

Table 3: Response time (recovery time) in seconds of sensors S1 (Conventional ZnO) and S2 (Porous Nanosolids) at 370°C and 420°C. [33]

Some of the current research work in the field of gas sensors focuses on CNTs for their novel properties like ballistic transport mechanism for detecting low concentrations of analytes, ability to be functionalized and decorated with metal nanoparticles [38] for improving selectivity and sensitivity. The proposed sensing mechanism [34] involves the physisorption of the analyte molecules on the CNTs resulting in a net change in resistance of the sensing film. The sensitivity of CNT based gas sensors can also be defined using Eq [1] above. Some researchers have also reported the impact of introducing defects like vacancies and stone wall defects on CNTs in order to enhance sensitivity to gases like NO_2 and NH_3 [39]. These defect sites lower the activation energy barrier thus enabling chemisorption of analytes on the surface of CNTs and makes room temperature measurements possible. Sensitivity of CNTs to gases like Oxygen (O_2) [40], NO_2 [41], NH_3 [38], H_2 [42], Water (H_2O) [43], Carbon Dioxide (CO_2) [40] and Nitrotoulene [44] has been reported at room temperature and are as shown in Table 4. A

quick comparison of results in Table 4 to the results reported for ZnO to Table 3, shows the lower operating temperatures for CNT based gas sensors as discussed in previous sections.

CNTs Used	Analyte	Temperature	Concentration	Response Time
S-SWNT	O_2	25 °C	O_2 (80 %)	15 Min
S-SWNT	NO_2	25 °C	200 PPM of NO_2	5 - 10 Sec
S-SWNT	H_2	25 °C	40 PPM of H_2	Instantaneous
MWNT + SiO2	CO_2	25 °C	10% CO_2	45 Sec
MWNT + SiO2	NH_3	25 °C	10% NH_3	2 Min
MWNT + SiO2	H_2O	25 °C	10% H_2O	4 Min
S-SWNT	NO_2	25 °C	44 PPB NO_2	Few Seconds
S-SWNT	NH_3	25 °C	1% NH_3	5 - 10 Sec

Table 4: Summary of the results reported for sensitivity of CNTs to different analytes

Functionalization of these CNTs with appropriate catalysts has shown increased sensitivity and selectivity for gases like NH_3 and NO_2 [45,46]. The CNTs used for gas sensing are reported to be mostly semiconducting [47,48,49,50] in nature; for the metallic CNTs there is only a small shifts of the Fermi level with the adsorption of the analyte on the surface of the CNTs. This does not result in a substantial change in the density of states at the Fermi level and, thus, in the charge carriers in the CNTs [46]. Recent developments in the synthesis of CNTs have made it possible to decorate CNTs with semiconducting metal oxides or metal nanoparticles (both inside and outside) which can be very useful for gas sensing measurements. Gabriel et al have reported chemical selectivity for different analytes by decorating the CNTs with different metal nanoparticles [38]. Differences in catalytic activity of catalytic metals like Pd [41], Pt [47], and Au [44] was observed for detection of gases like H_2, CH_4, CO, and H_2S.

1.4 Motivation

Researchers in the past have reported improvement in sensitivity for gas sensors by using nanostructured materials or catalysts; however less work has been reported on further improving the sensitivity of the gas sensors with the use of both nanostructured materials and catalysts. This was the motivation to fabricate highly sensitive gas sensors operating at room temperature by using both porous nano-structures and catalytic effects. Also, modeling the sensitivity as a function of the input parameters (process parameters, material properties and the device parameters) has attracted little attention over the years. This should be helpful to design the sensors platforms and experiments in order to achieve an optimum response. A designed experiment in order to understand the effects of these parameters and the interaction effects will be conducted in order to model the sensitivity of these sensors. This would help to simulate the sensitivity of a sensor before actually running the experiments which should in-turn save resources in terms of time and money.

Most results of high sensitivity using CNTs are obtained by using commercial grade CNTs, which makes it difficult to relate the sensitivity to the properties of the material used. However, using CNTs grown in-house at the Nanopower Research Labs would be an opportunity to model the sensitivity of the CNTs as a function of their chirality and size (length and diameter). Also the capability of the Nano-Power Labs to produce higher quality tubes would be used to conduct a detailed study on the effect of purity of CNTs on sensitivity to different gases. This would not only help to provide an in-depth understanding of sensing mechanism but will also segregate the effect of impurities.

1.4 Organization of this Dissertation

Chapter II gives an overview of the gas sensor system setup and sensor fabrication with emphasis on material characterization gas sensor design. The basic material characterization techniques for both ZnO and CNT based nano-materials are discussed. Fabrication details for both single and dual level MEMS gas sensors are presented in addition to the process details. The chapter further discussed gas sensor setup and details of the bubbler circuit. Finally details for different sets of experiments are presented. This includes experiment details of resistive measurements for ZnO and CNT based nano-materials, DOE study for ZnO nano-platelets and impedance spectroscopy for HiPCo produced SWCNTs.

Chapter III discusses the results obtained for different experiments. Highly sensitive gas sensors based on ZnO nano-platelets are presented. Saturation in sensitivity values observed at higher concentration of the analytes is correlated to Langmuir's theory of adsorption isotherms. Catalytic effect of platinum is demonstrated for ZnO sensors with H_2. The sensitivity of the sensor is also modeled as a function of device and process parameters. Finally, results of the DOE study with focus on the interaction effects between different process and device parameters are also presented.

Results for CNT based nano-materials to different gases and organic solvents are presented in Chapter IV. Results for both resistive and impedance spectroscopy based gas sensors are discussed. Sensitivity of ZnO and carbon nanotubes based nano materials are also compared for various analytes.

Chapter V is general conclusion section also including recommendations for future work.

CHAPTER II

GAS SENSOR FABRICATION AND EXPERIMENTAL DETAILS

2.1 Sensor Design

2.1.1 Commercial Sensors

Both commercial and in-house fabricated micro-machined (MEMS) gas senor platforms were used for the sensing measurements. The commercial gas sensor platform was Heraeus - MSP632 which consisted of a temperature sensor (Pt-1000), a heater and inter-digitated electrodes. The spacing between the inter-digitated electrodes was 10 μm in platinum thin film. Fig 8 shows both the top view and the schematic of the sensor head MSP-632. A ceramic substrate was used as a base for the temperature sensor and the heater. The inter-digitated electrodes were over a glass base which was used to insulate the electrodes from the heater and the temperature sensor.

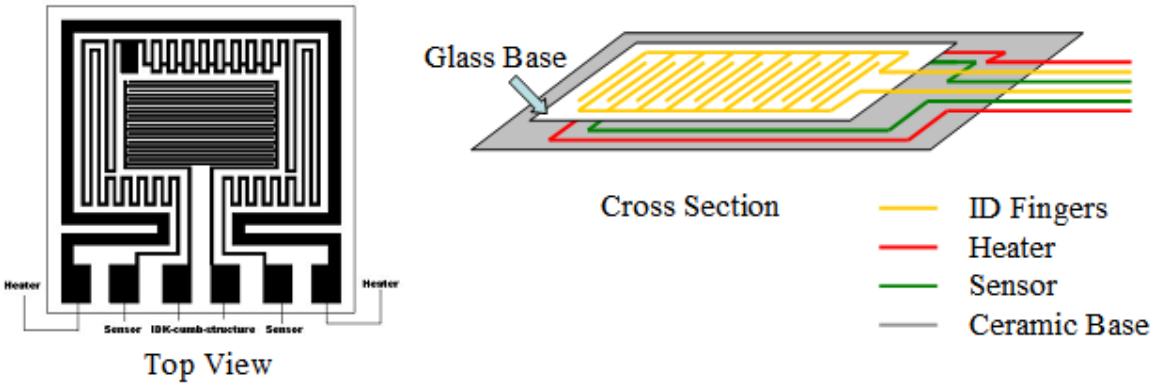

Fig 8: Shows Top View of MSP-632 (Left), Schematic of Heraeus MSP-632 (Right)

Heraeus MSP-632 sensor head was chosen over its other counterparts as it had Platinum heater and temperature sensor. Platinum is advantageous over other metals as it can maintain stability even at higher temperatures. The temperature sensor of the MSP-632 was characterized in order to regulate the temperature of the heater accurately. Resistance of the temperature sensor was measured for different temperature readings of the furnace. These values were then used to model the dependence of resistance on temperature. The equation showing the dependence of resistance on temperature is as shown in Eq 2.

$$R\ (\text{Ohms}) = 3.2252 * T\ (^{o}C) + 991.36 \qquad \text{Eq 2}$$

where 991.36 is the resistance of the heater at 0^{0}C and 3.2252 is the experimentally determined value of α_o where α_o is the temperature coefficient of resistance. Fig 9 shows resistance v/s temperature for the sensor head. Resistance values recorded at specific temperature settings were used to calculate the temperature coefficient (α) of platinum.

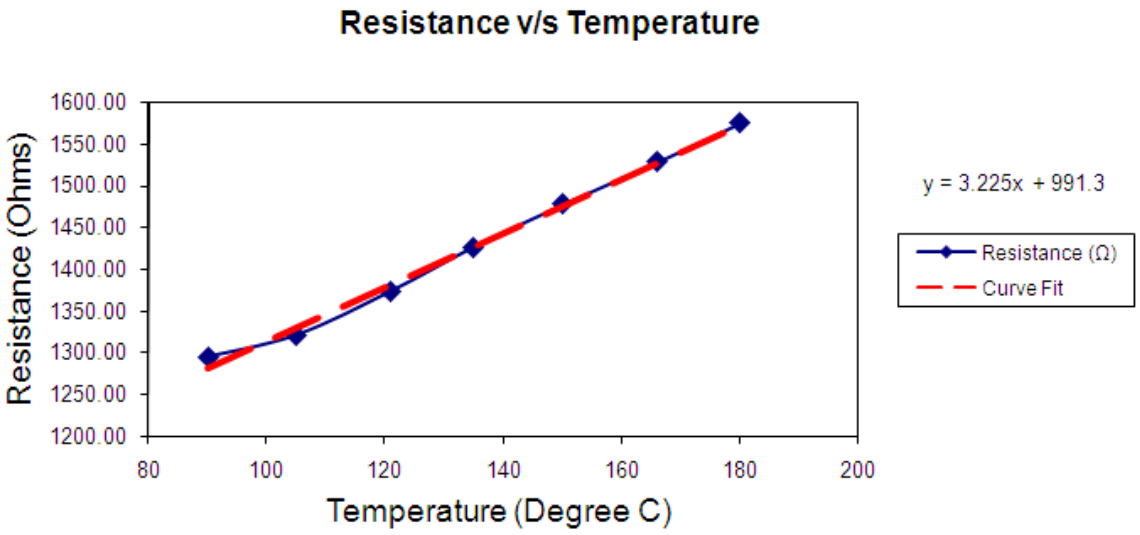

Fig 9: Graph for the resistance values attained at specific temperature settings.

The commercial sensor head was used for the initial results of the ZnO based and SWCNT based gas sensors. However, the sensitivity of a gas sensor can vary as a function of various parameters. These parameters can be categorized as process parameters such as temperature, concentration & carrier gas flow; material properties such as morphology & surface area and device parameters such as inter electrode spacing & number of electrodes. The affect of these factors on the sensitivity, response time and recovery time can be hypothesized as in Table 5. Detailed experiments were designed in order to evaluate the response of these factors on the sensitivity. However, in order to vary the device parameters, MEMS sensors were designed and fabricated in-house. The following section discusses the design of the MEMS sensors for this study.

Factors	Sensitivity	Response Time	Recovery Time
Heater Temperature	High	High	High
Concentration	Intermediate	Intermediate	Low
Inter-Electrode Spacing	Intermediate	High	High
# of electrodes	High	Low	Low
Catalyst	High	High	Low
Voltage Bias	Intermediate	Intermediate	Intermediate
Carrier Gas Flow	Intermediate	High	High

Table 5: Summary of factors affecting the response of the sensor.

2.1.2 MEMS Based Sensors

As mentioned before, MEMS based sensors were designed and fabricated in order to analyze the effect of device parameters on gas sensitivity. The inter electrode spacing & number of electrodes were varied on these devices. Fig 10 shows schematics of various devices designed for MEMS fabrication.

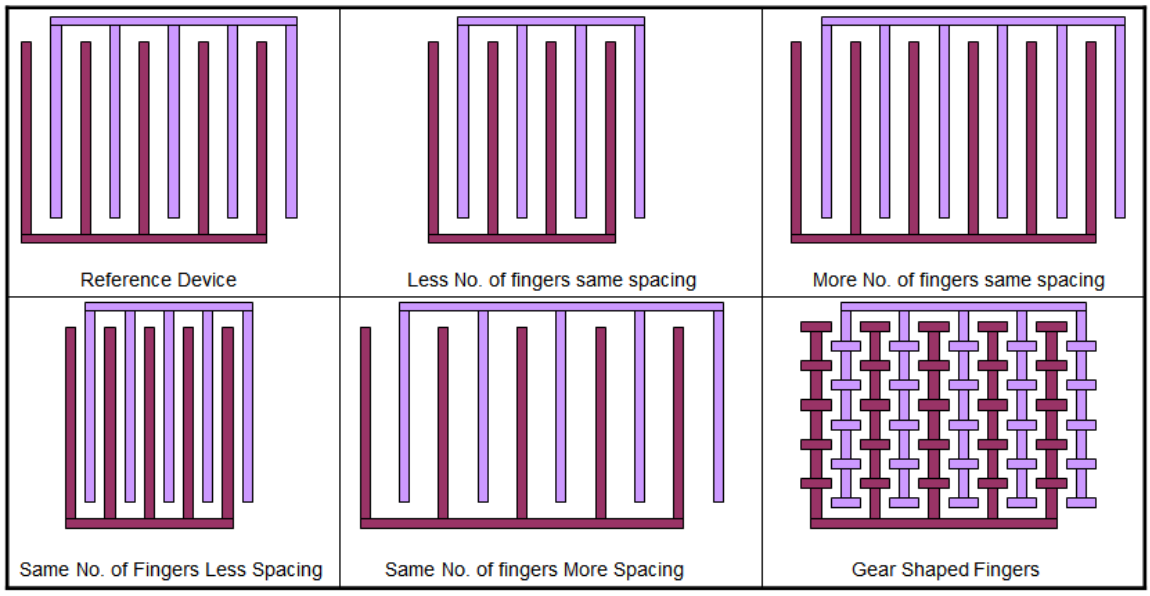

Fig 10: Schematics of various devices designed for MEMS fabrications.

The design of these devices was based on one factor variation. The reference device was designed to have 20 inter digitated electrodes with 20 micron spacing between the electrodes. The number of fingers was varied to 10 and 30 for two devices respectively with the same spacing of 20 microns between the electrodes. This was to understand the affect of more electrodes (hence more surface area on gas sensitivity). Also, spacing of two different devices was varied to 10 and 30 microns respectively in order to understand the affect of spacing on gas sensitivity. In addition to the five devices

mentioned, the sixth device had gear shaped fingers where the distance between the two gears was as less as 6 microns with 20 electrodes. Table 6 gives the specifications of the designed devices.

Device ID	Device Specifications	
	Spacing	# of Fingers
1	20 Microns	20
2	20 Microns	30
3	20 Microns	10
4	10 Microns	20
5	30 Microns	20
6	6 Microns	20

Table 6: Device Specifications of the MEMS based gas sensors.

The two level MEMS sensors were designed to have a platinum heater and temperature sensor above the diaphragm as the first level, with inter digitated electrodes defined by the second level metal. Wherein, the two metal levels were separated by an interlevel di-electric. Fig 11 shows the layout and cross-section of the reference device. The total area surface area covered by the IDEs was 2500 µm X 2500 µm.

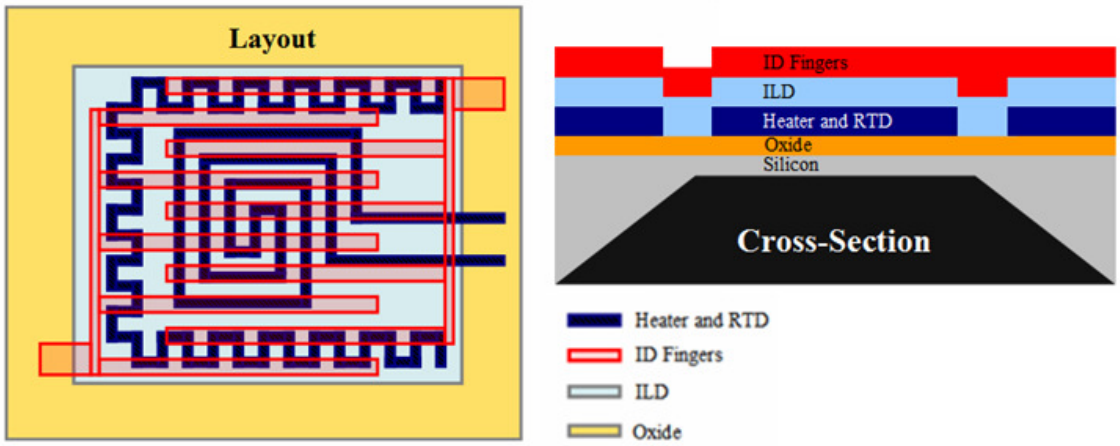

Fig 11: Shows Layout (left) and Cross-Section (right) of the MEMS gas sensors.

Both commercial and MEMS sensor heads were fabricated and tested as gas sensors. Fabrication of commercial sensor heads as gas sensors involved depositing uniform films of different analytes (ZnO and CNT based nano-materials). For MEMS based gas sensors, sensor heads were first fabricated using standard processing techniques, following which, uniform films were deposited using various techniques. The following section discusses sensor fabrication in detail.

2.2 Sensor Fabrication

2.2.1 Commercial Sensors

Different methods were deployed to fabricate gas sensors depending on the sensing material. As mentioned above, these sensing materials were ZnO based nano-materials, nano-particles and web like films and SWCNTs – arc produced and HiPCo tubes. The following paragraphs elaborate on the various methods used for gas sensor fabrication with the foresaid materials.

For ZnO based nano-materials, each sample (30% by weight) was individually mixed with 100% α-terpineol - which acts as a binder because of its viscous nature [23] - and sonicated for 30 min. The resulting solution was drop casted over different sensor platforms and allowed to dry for 30 min at 100 ^{o}C in order to evaporate the α-terpineol and form a uniform film. Sensitivity of these different sensors was then recorded for various analytes. The uniformity of the film formed, was investigated under the F-SEM and is discussed in more detail in the following sections.

Commercial sensors were also fabricated as gas sensors using arc produced tubes. For this, (1.2 X 10^{-5} gm/ml) were dispersed in Dimethylamine (DMA) and sonicated for 3

hours, after which 10 µl of the solution was drop casted over the MSP-632 sensor platforms. These sensor platforms were then subjected to heat at about 80 ^{o}C to evaporate the solvent. Owing to the high conductivity of the CNTs a semiconducting behavior was achieved only by using a very small concentration. This limits the surface area for gas sensing which could be increased if a semiconducting behavior could be achieved even by increasing the concentration of the tubes. For this, MEMS gas sensors were used with the HiPCo produced SWCNTs. The details of sensor fabrication with HiPCo tubes are described in the following section.

2.2.2 MEMS Based Sensors

MEMS based gas sensors were fabricated at Rochester Institute of Technology in two phases. Single level sensors using inter-digitated fingers for gas sensing at room temperature were fabricated in the first phase. This approach was followed as the single level sensors were low cost and had a shorter cycle time which helped in getting sensitivity results sooner. Standard processing steps like oxide growth, evaporation and lift off techniques were used in the fabrication.

The following discusses the fabrication of the single level sensors in detail. P-type [100] 4" silicon wafers were used as starting substrates and a 5000 A thick oxide layer was grown to isolate the first level metal from the substrate. Following the oxide growth, Lift-off Resist LOR-5A was spin coated on the substrates for Pt/Cu lift-off. The thickness of the resist coated was estimated using the spin curve for the LOR-5A. The bake times of the LOR-5A were optimized in order to obtain faster lateral etch at the time of lift-off. A layer of positive photoresist (Shipley 1813) was then spin coated for photolithographic

process. Karl Suss Mask Aligner (MA-150) was then used to expose the wafers for the first level lithographic step with an exposure dose of about 156 mJ/cm^2. The wafers were then developed using a CEE-100 developer. The develop time was calculated to be about 2 min in order to ensure formation of undercuts for the metal evaporation. Before Pt or Cu deposition, 50 Å of Titanium metal was used as an adhesion layer to ensure adhesion of Platinum to the underlying oxide. The thickness of the electrode metal was chosen to be about 500 nm to ensure lift-off. The wafers were then sub-merged in Nano-Remover PG for about 15 min for lift-off. Fig 12 demonstrates the flow of the fabrication process described above.

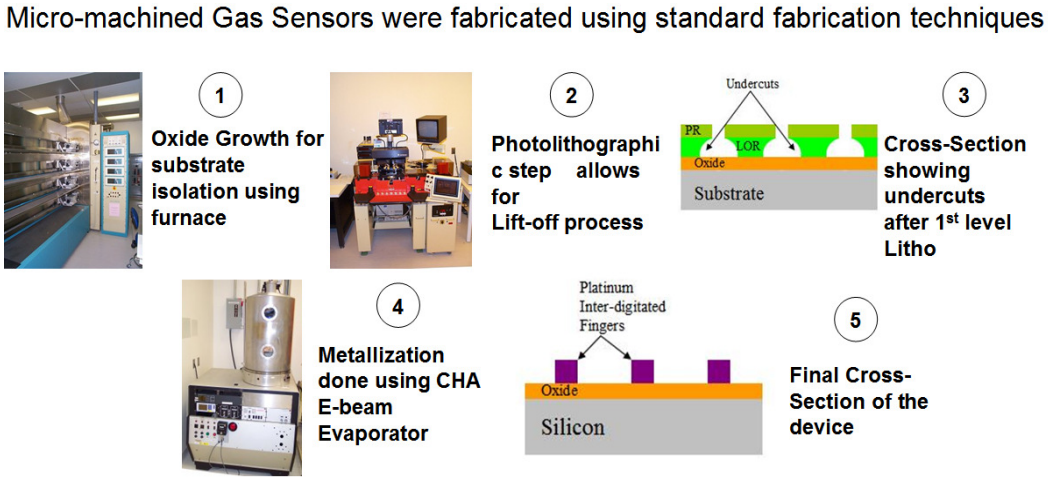

Fig 12. Showing the steps followed for fabrication of single level sensors.

Completed wafers were diced using a Tempress 4 inch wafer saw for making connections and gas sensor fabrication. Platinum and Copper were chosen to enhance the sensitivity of ZnO to H_2 and CO respectively for to their catalytic properties. As mentioned in previous sections, sensors having different inter-electrode spacing (6, 10, 20, 30 μm) with 20 pairs of electrodes and different number of electrodes (20, 40, 60) with 20 μm spacing were fabricated to study the effect of inter-electrode spacing and

number of electrodes on gas sensitivity. Effective area on chip for gas sensing was 2500 μm x 2500 μm. An optical and scanning electron micrograph of the diced chip is shown in Fig 13.

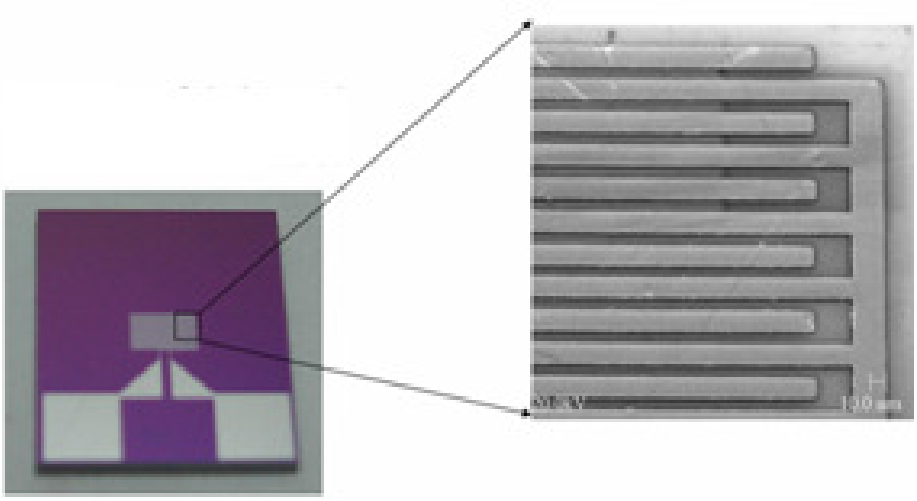

Fig 13: Optical image of in-house fabricated single level MEMS sensor (inset shows SEM image of IDTs)

In addition to the single level MEMS based gas sensors; an effort was made to fabricate dual level sensors during the second phase of fabrication. The full details of fabrication and the process flow are given in the Appendix.

These MEMS sensor platforms were then fabricated as gas sensors using both ZnO and HiPCo produced tubes. The gas sensor fabrication process using ZnO nano-particles was exactly the same as discussed above for commercial sensors and is mentioned her for the reader's convenience. ZnO based nano-materials were mixed with 100% α-terpineol and sonicated for 30 min. The resulting solution was then drop casted over different sensor platforms and allowed to dry for 30 min at 100 ^{o}C.

As-received SWCNTs, fabricated using the HiPCo process were also used in this work to analyze the gas sensing response of CNTs to various analytes. However, as

discussed before for Arc produced carbon nano-tubes, due to the high conductive nature of the tubes, only a small amount of tubes could be used for fabricating commercial sensor heads as gas sensors. In order to overcome this limitation, MEMS sensor heads were cleaved to use only the Pt bond pads as the electrodes. In this case the two electrodes were 2.5 mm apart instead of 10 μm as in commercial sensors. Following this, the SWCNT sample (2.5 mg) was mixed with 100 microlitres (ul) of tetramethylmalonamide (TMMA) and sonicated for 30 min to form a thick paste. This paste was screen printed between the Pt bond pads and allowed to dry for 30 min at 100 ^{o}C to form a uniform film.

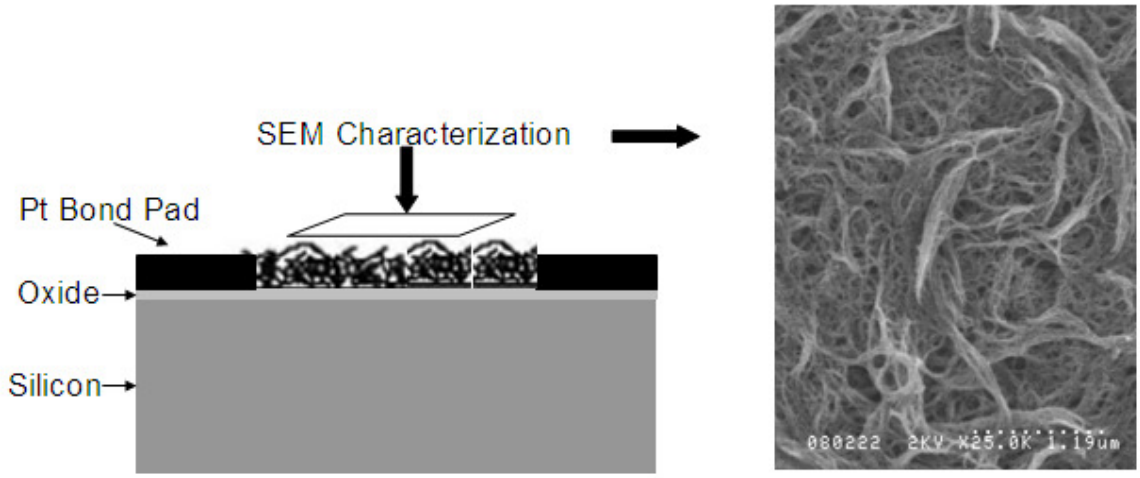

Fig 14: (a)Cross-section of the gas sensor along the bond pads. (b)SEM image of as-received HiPCo SWCNT network

A cross-sectional schematic of the fabricated gas sensor is shown in Fig 14(a). As-received HiPCo SWCNT samples were studied using a Hitachi N-900 Field Emission SEM. Fig. 14(b) shows the SEM image of these SWCNTs used for gas sensor fabrication. A uniform film of SWCNTs was observed between the platinum electrodes under the SEM.

2.3 The Gas Sensor System Setup

The gas sensor setup was built at Rochester Institute of Technology to measure the sensitivity of ZnO and SWCNT based nanostructures to different gases and organic solvents. Fig 15 shows the schematic representation of the setup. Gas sensing was performed in a closed quartz chamber and the flow of gases was regulated using calibrated mass flow controllers (MKS 1179) having an accuracy of 2.5% of full scale and a settling time of less than 2 seconds to within 2% of set-point. Nitrogen gas ($N_{2)}$) was used as a carrier for all the sensing measurements. The limit of the mass flow controller used to monitor the flow of the carrier gas was 20 standard liter per minute (SLM), whereas, the limit for the mass flow controllers used for the sensing gas were chosen to be 200 standard cubic centimeter per minute (SCCM).

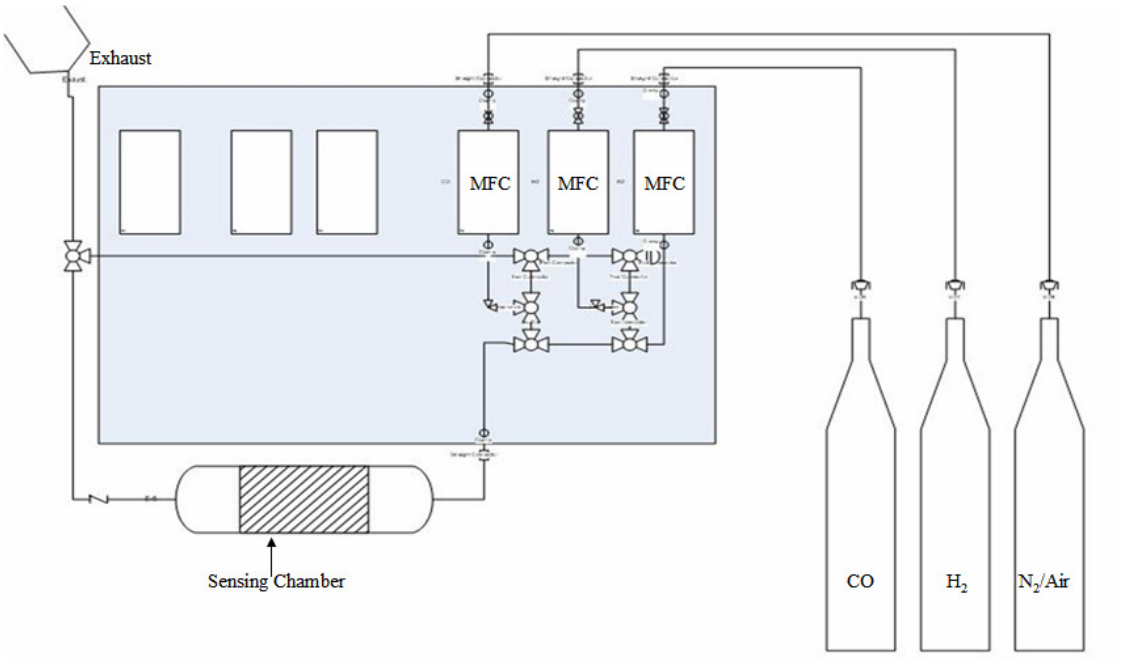

Fig 15: Schematic of the Gas Sensor Circuit.

Fig 16: As Built Gas Sensor Circuit

Fig 16 shows the as built gas sensor circuit for direct comparison to the designed circuit. As mentioned before the gas lines were fed to the sensing chamber from the gas bottles via the mass flow controllers. The output from the sensing chamber was fed to the exhaust as shown in the upper left corner in Fig 16.

The sensing gases used were commercially bought from Airgas with a concentration of 2% analyte balanced with N_2, where the analyte was Hydrogen (H_2), Carbon Monoxide (CO) and Ammonia (NH_3) in three different gas bottles respectively. Proper mixing of sensing gas with the carrier gas was ensured by merging the gas lines before the input to the gas sensing chamber. The concentration of the analyte in the chamber was calculated using the Eq 3.

$$C = \frac{Q_{analyte} \text{ X } 10^6}{Q_{N2}} \qquad \text{Eq 3.}$$

where C is the concentration of the analyte in PPM , $Q_{analyte}$ and Q_{N2} are the flows of analyte and N_2 in the chamber respectively. $Q_{analyte}$ was calculated to be 2% of the flow of sensing gas and Q_{N2} was calculated as the sum of flow of carrier gas and 98% of the flow of sensing gas.

The change in current was monitored with respect to time using a Keithley-236 source measure unit interfaced to the computer through a Lab-View program. Also, a Agilent B1500 parametric analyzer was used to measure the impedance of the SWCNT based sensor for impedance spectroscopy measurements. The recorded data was then used to evaluate the response of the sensor to the various analytes.

The sensitivity of SWCNT based sensor was also measured for different organic solvents like Methanol (CH_3OH), Ethanol (C_2H_5OH), Water Vapor (H_2O), Di-methyl Amine (DMA), and Isopropyl Alcohol (C_3H_8OH). In order to introduce these solvents to the sensing chamber, N_2 was first bubbled through the liquid organic solvents. Fig 17 shows a schematic of the bubbler circuit used to feed the analyte rich N_2 gas to the sensing chamber. The pressure of N_2 in the bubbler was maintained with the help of an upstream gas flow regulator at 5 Psi for all the measurements. The output from the bubbler circuit was then fed as the input to the downstream mass flow controller – used to maintain the flow of sensing gas (analyte rich N_2) in the chamber (as in Fig. 17).

The molar flow (M) of the solvent in the output of the bubbler circuit was calculated based on its vapor pressure at room temperature using Eq 4 where Q is the flow of N_2 through the circuit, P_T is the total pressure of the system and P_V is the vapor pressure of the solvent at a given temperature and is defined as the pressure at which a gas is in dynamic equilibrium with its solid or liquid phases indicating equal evaporation

and condensation of the species. The pressure in the bubbler was held constant at 5 Psi throughout the measurement in order to maintain same flow in the chamber.

$$Q_{analyte} = Q_{N2} * \frac{P_V}{P_T} \qquad \text{Eq 4.}$$

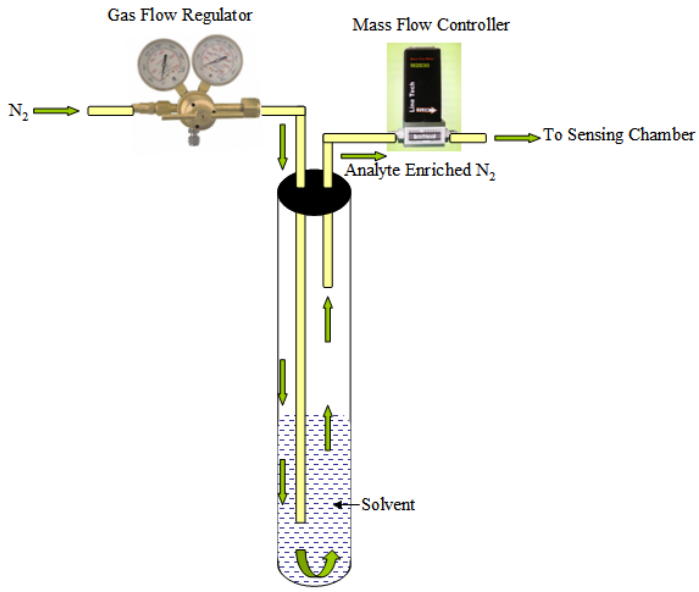

Fig 17. Schematic of Bubbler Circuit.

For all experiments, the carrier gas was high purity N_2 and dry industrial air was used after exposure to recover the sensors to their initial state. Gas flow for the carrier gas and recovery gas were kept high (2.5, 5 and 10 standard liters per minute (SLM)) to achieve shorter response and recovery times where the response time and recovery time can be defined as the time taken for the sensor to reach up to 90% of the final value.

In order to determine the approximate time taken by the analyte to reach the sensor, the gas velocity was calculated using the ideal gas law. This value of gas velocity

was then used to determine the approximate time taken by the sensor to respond once introduced to the analyte. Typical values of gas velocities calculated for different gas flows are as shown in Table 7. The velocity of the gas depends on the geometry of the system hence all further discussions will be in terms of the flow of the gas.

Total Flow (SLM)	Gas Velocity cm/sec	Time Taken to Reach the sensor (Sec)
2.5	1.04	38.63
5	2.07	19.32
10	4.14	9.66

Table 7: Values for calculated gas velocity over the sensor and time taken by the analyte to reach the sensor.

2.4 Experimental Details

Preliminary work involved analyzing the sensitivity of the ZnO based nano-materials towards H_2 gas using the MSP-632 sensor heads. Different experiments showed repeatability and reproducibility of results. Further experimentation was carried out to confirm effect of temperature, carrier gas velocity and catalytic effect – (platinum v/s copper electrodes) on sensitivity of these nano-materials. Based on the initial results with H_2 gas, a DOE (Design of Experiments) study was carried out for ZnO nano-platelets using the MEMS based gas sensors, to understand and model the sensitivity as a function of device and process parameters. Following this, sensitivity of ZnO nano-platelets was also recorded for other gaseous analytes and organic solvents at an operating temperature of 200^{o}C. Sensitivity for all experiments with ZnO based nano-materials was calculated

by measuring resistance – at constant voltage bias- before and after exposure to the analytes.

For carbon nano-tubes, initial measurements were carried out for arc produced tubes with different gaseous analytes and organic solvents using the commercial sensors MSP-632 sensor heads. As for ZnO based nano-materials, sensitivity was calculated by measuring resistance before and after exposure to the analytes at an operating temperature of 200^{o}C. However, as higher concentration of the tubes resulted in shorting of the inter-digitated electrodes, extremely low concentration of the arc produced tubes was used for fabricating sensor heads. This limits the sensor capability and decreases the signal to noise ratio for low concentrations of the analytes.

In order to overcome the limitations encountered for sensors fabricated with arc produced tubes, impedance spectroscopy was implemented using MEMS based gas sensors fabricated with HiPCo tubes. As the resistance of the SWCNTs is not independent to the frequency of the applied AC signal, Impedance Spectroscopy was implemented to analyze the gas sensitivity as the charge transferred to the SWCNTs on reaction with the analytes is used to determine the sensitivity. Appreciable results were recorded at room temperature for these tubes with Impedance Spectroscopy. The following sections describe the different experimental procedures carried out with different sensing materials and analytes in detail.

2.4.1 ZnO Based Resistive Sensors

For preliminary results, gas sensing measurements were performed for different concentrations of the analyte (H_2) at various carrier gas (2.5 SLM, 5 SLM and 10 SLM)

flows and different operating temperatures (25^{o}C, 150^{o}C). Incomplete recovery of the sensor was observed at room temperature, supposedly due to the formation of water as a bi-product of the reaction on the surface of the sensing film. Measurements at 150^{o}C confirmed that the formation of water on the surface of the sensing film causes this incomplete recovery of the system. The temperature was controlled by keeping the resistance of the Pt-1000 constant at 1475 ohms corresponding to a temperature of 150^{o}C. These calculations were based on Eq 2 mentioned before. Measurements at higher carrier gas velocities were performed to understand the effect of carrier gas on response and recovery of the system. Shorter response and recovery times were expected with higher carrier gas velocities.

For all the measurements, the sensors were allowed a stabilization time of 100 seconds in N_2, followed by exposure to the sensing gas for 200 seconds which was followed by another stabilization time of 100 seconds in N_2 prior to a recovery of 200 seconds in dry industrial air. Sensing gas was mixed with the carrier gas before flowing in the quartz chamber. Owing to the short response time required for some industrial/space applications and high sensitivities observed in the previous experiments, short exposure time of 200 seconds was chosen to measure the response of the sensor to the analytes.

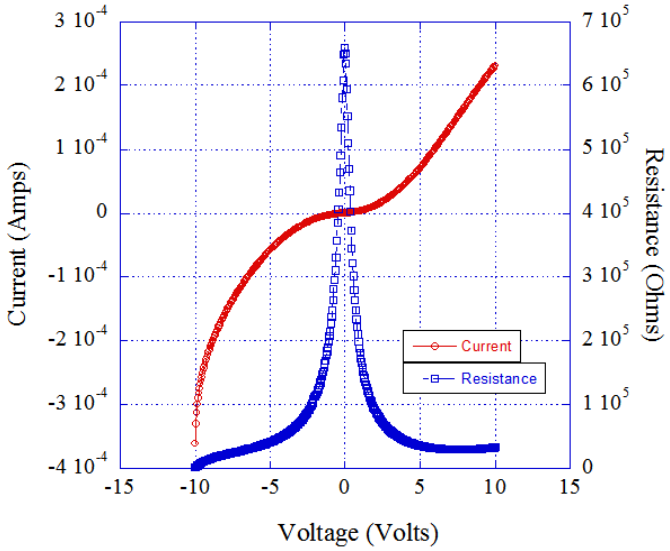

Fig 18. Showing I-V sweep and R-V sweep for ZnO nano-platelets

In order to determine the appropriate voltage bias to be applied across the sensor for a maximum signal to noise ratio, the current was measured across the IDEs for different values of voltages. Fig 18 shows an I-V sweep for the ZnO nanoplatelets showing the semiconducting behavior of the metal oxide. This data was then used to calculate resistance, for all values of current at specific voltage intervals using ohms law. A plot of resistance versus voltage was then used to choose the voltage bias of 5 Volts to be applied in order to maximize the signal to noise ratio.

Unlike H_2, ambient conditions were modified for measurements with some analytes gases (O_2 and NH_3). This was done to ensure recovery of the sensor back to a stable condition. For O_2, a continuous flow of 400 PPM H_2 (with N_2 as the carrier gas) was introduced in the chamber and the sensor was allowed to saturate. The resistance of the sensor at saturation - while exposed to 400 PPM H_2 - was then considered as the initial resistance. The sensor was then exposed to O_2, while the flow of H_2 was

maintained in the chamber. The presence of H_2 in the chamber ensured full recovery of the sensor to its initial state. For NH3, industrial air was used as the carrier gas for both the response and recovery phase. Measurements were carried out with the same exposure and stabilization time for all the experiments.

2.4.2 Design of Experiments

The effect of different process and device parameters was recorded for ZnO nano-platelets with H_2 gas. The device parameters considered for the experiments were spacing between the electrodes and the number of electrodes. Whereas, voltage bias across the electrodes, concentration of the analyte and the operating temperature were the process parameters for the experiments. Table 8 below shows the different parameters and their range of variation. All the parameters were varied from the lower limit to the upper limit in regular intervals. Three levels of variation were considered for all the parameters except for concentration of the analyte, which was varied in five different levels. In-house fabricated single level MEMS based gas sensors were used for this study. In order to take measurements at higher temperatures, namely (75^{o}C and 125^{o}C) these single level MEMS sensor heads were physically glued to the MSP-632 sensor heads using thermally conducting epoxy OB-100, and allowed to dry overnight at a controlled temperature of 80^{o}C.

Effect of SPACING				Effect of # of ELECTRODES			
Parameter	**Lower Limit**	**Upper Limit**	**Units**	**Parameter**	**Lower Limit**	**Upper Limit**	**Units**
Spacing	10	30	Microns	# of Electrodes	20	60	
Bias	5	10	Volts	Bias	5	10	Volts
Concentration	20	60	PPM	Concentration	20	60	PPM
Temperature	25	125	Degree C	Temperature	25	125	Degree C

Table 8: Different parameters and their range of variation for the DOE study.

As mentioned above, the DOE study was carried out only with H_2 gas as the analyte and the experiments were also conducted in a similar manner. The experimentation details are mentioned below for convenience of the reader. For all the experiments, sensors were allowed a stabilization time of 100 seconds in N_2, followed by exposure to the sensing gas for 200 seconds which was followed by another stabilization time of 100 seconds in N_2 prior to a recovery of 200 seconds in dry industrial air.

Initial results for the DOE study showed promising results. However the effect of concentration on sensitivity was suppressed by the high temperature. In order to understand the effect of each parameter, a separate set of experiments were performed to record the sensitivity of the nano-platelets at room temperature. Table 9 shows the factors considered for this set of experiments. The results of the DOE study are discussed in detail in Chapter III.

Effect of SPACING				Effect of # of ELECTRODES			
Parameter	**Lower Limit**	**Upper Limit**	**Units**	**Parameter**	**Lower Limit**	**Upper Limit**	**Units**
Spacing	10	30	Microns	# of Electrodes	20	60	
Bias	5	10	Volts	Bias	5	10	Volts
Concentration	20	60	PPM	Concentration	20	60	PPM

Table 9: Parameters and their range of variation for the revised DOE study.

2.4.3 Carbon Nano-Tubes Based Resistive Sensors

An irreversible response of the CNTs was observed for some, but not all, of the analytes. This may be because of the chemisorption of the analyte on the CNTs. In order to ensure complete recovery of the sensor the ambient conditions of the chamber were modified as for ZnO based nano-materials with O_2 and NH_3. In this case, a continuous flow of 400 PPM O_2 was introduced in the chamber and the sensor was allowed to saturate. The resistance of the sensor at saturation - while exposed to 400 PPM O_2 - was considered as the initial resistance. The sensor was then exposed to the analyte, while the flow of O_2 was maintained in the chamber. The presence of O_2 in the chamber ensured full recovery of the sensor to its initial state. A voltage bias of 2V across the inter-digitated electrodes was applied to measure the gas sensing response. The operating temperature for all measurements with CNTs was kept constant at 200^{o}C as the CNTs did not show any response at room temperature and at an operating temperature of 100^{o}C. This was consistent with reports by other researchers [51] on gas sensing properties of arc produced CNTs.

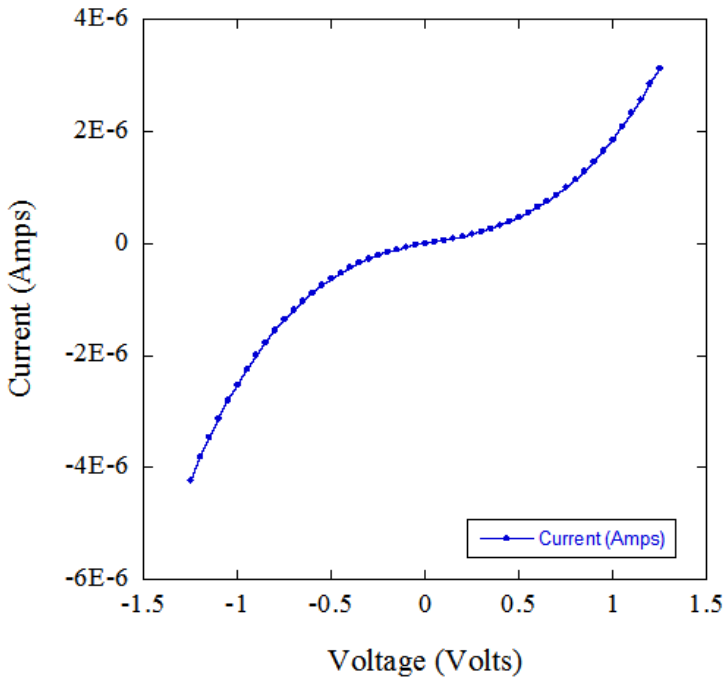

Fig 19: I-V Sweep of arc produced CNTs at 200°C.

Fig 19 shows current on the order of micro amps for the arc produced tubes; the current was recorded by sweeping the voltage across the inter-digitated fingers. High resistance with the arc produced CNTs was observed owing to the small quantity of tubes used for sensor fabrication. The I-V sweep was measured at a temperature of 200°C which was the operating temperature for the sensing measurements. The voltage bias across these electrodes for the final measurements was chosen to be 2V in order to increase the signal to noise ratio. Very small current on the order of micro-amps was observed for the small quantity of the tubes used for the sensor fabrication.

2.4.4 Impedance Spectroscopy Based Measurements with Carbon Nanotubes

Impedance spectroscopy was implemented using MEMS based gas sensors fabricated with HiPCo tubes, in order to overcome the limitations encountered for sensors fabricated with arc produced tubes. For this technique, the impedance of the sensor was measured over a given frequency range (1KHz – 1MHz). Nyquist plots were used to determine the response of the sensor to the analytes. Following sections discuss the circuit model and equivalent circuit in detail.

Gas sensing measurements were performed for the SWCNT network by varying exposure time and concentration to understand the effect of longer exposure times on sensitivity and estimate the lowest concentration of the analyte that can be detected. Sensitivity of SWCNT network to different analytes was determined by measuring the sensors impedance using an Agilent B1500 parametric analyzer. The response was measured at room temperature over a frequency range of 1 KHz to 1 MHz with a voltage bias of 2.5V across the electrodes.

A twofold approach was adopted in order to understand the gas sensing response of the SWCNT network to different analytes. This was done by recording the sensitivity of the sensor to varying exposure time and varying the concentration of the analytes in two different sets of experiments. For studying the effect of varying exposure times, sensors were exposed to high concentrations of analytes. This was about 2.04% for analytes in gaseous forms; however, concentration of organic solvents depended on the vapor pressure and was different for every solvent. For organic solvents; N_2 was bubbled through the liquid at a constant pressure of 5 PSI before being mixed with the carrier gas.

The molar flow (M) of the solvent at the output of the bubbler circuit was calculated based on Eq 4. The sensor was exposed to each analyte for a total duration of 25 Min, wherein the response of the sensor was measured at regular 5 Min intervals.

Sensitivity values were also recorded while varying the concentration of the analytes. For this, the sensor was exposed to a specific concentration value of the analyte for a period of 5 minutes before measuring the impedance, after which the concentration of the analyte was increased and the sensor was allowed to saturate in this increased concentration for a period of 5 minutes before measuring the sensitivity for the second time. The above process was repeated for various concentration values in order to record the response of the SWCNTs to these concentration levels.

In the recovery phase, industrial air was used to drive the vapors of the sensing gas out of the chamber, after which the sensor was allowed to recover in room ambient over a period of 4 to 6 hours depending on the chemisorbed analyte. All measurements were carried out at room temperature.

CHAPTER III

ZnO Nano-Structures Based Gas Sensors

3.1 Material Synthesis and Characterization

Gas sensors were fabricated at R.I.T using different nano-materials, in order to evaluate the sensitivity to different analytes as a function of their material properties. ZnO based nano-materials, namely Nano-Platelets (commercially bought ZnO based nano-material) and Web like films (prepared by collaborators at Miami University of Ohio) were analyzed for this study. This section discuss the synthesis techniques, material characterization and gas sensor fabrication carried on these samples for gas sensor fabrication.

ZnO commercial samples (nano-platelets), bought from Sigma Aldrich Inc. were used to fabricate gas sensors for measuring the response to different analytes. ZnO nano-platelets (S1) were prepared by dissolving the ZnO nanoparticles whereas ZnO web-like films (S2) were prepared at Miami from chemical bath deposition. The chemical bath was prepared from 15 ml of 0.15 M zinc acetate dihydrate ($Zn(CH_3COO)_2 .2H_2O$, Sigma-Aldrich, 98%+) in a methanol solution. After deposition for 30 hours at 60°C, the as-synthesized films were annealed at 200°C for 5 min and then 450°C for 15 min [52].

The morphology and the surface area of the ZnO nano-platelets (S1) and ZnO web-like films (S2) were determined by studying the samples under the F-SEM and BET, respectively in order to relate sensitivity to material properties. To study only morphology, the ZnO particles were suspended in ethanol and drop cast on conductive

carbon tapes, a thin discontinuous film of platinum was then sputtered over the sample, which was then inspected using a Hitachi N-900 Field Emission Scanning Electron Microscope (F-SEM). SEM images demonstrate formation of plate-like nanostructures and web-like films under different deposition conditions for S1 and S2 respectively, as shown in Fig 20. Thickness of the nano-platelets was estimated to be about 15nm from the SEM pictures whereas diameters of 5nm were observed for web-like films.

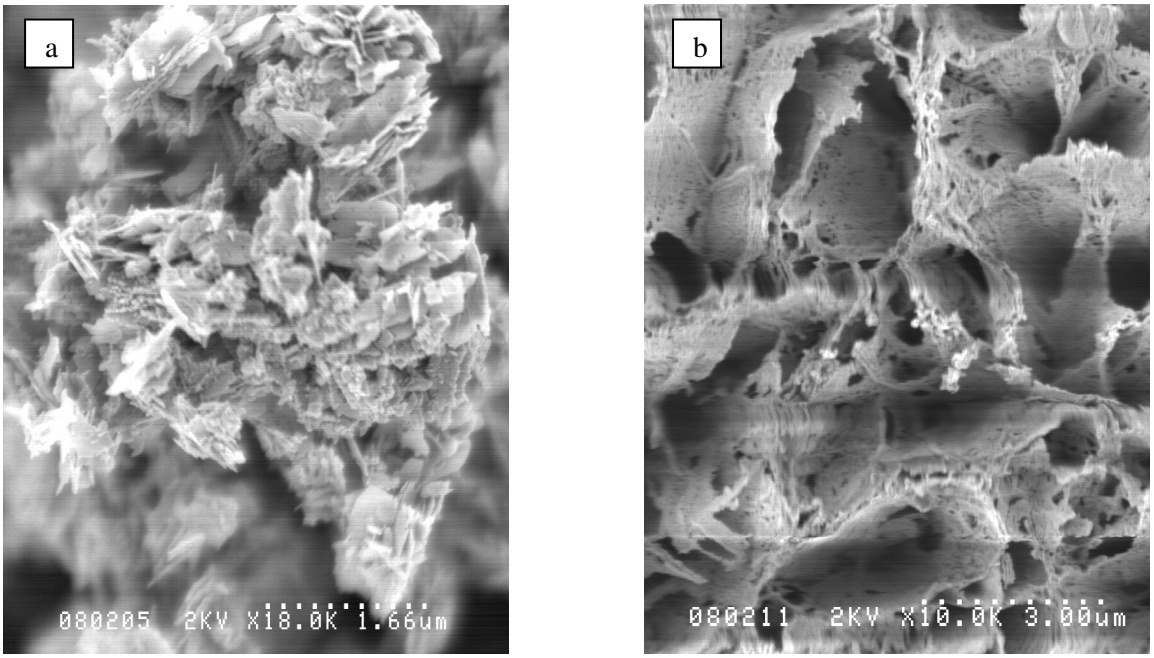

Fig 20: SEM images showing the morphology of a) ZnO nano-platelets and b) ZnO web-like films.

In order to determine a method to deposit uniform and dense films of ZnO particles, the morphological effects of both spin coating and drop casting were studied. Uniformity of the film for device application was investigated by suspending particles in different ratios of ethanol and α-terpineol, spin coating or drop casting on small pieces of silicon wafers, and analyzing the uniformity of the sensing film by F-SEM.

A concentration of the solution of 16.3 mg/ml was used for spin coated at 3000 RPM for 30 seconds on the samples with an initial speed of 500 RPM for 9 seconds and a ramp up time of 5 seconds. Platinum was then sputtered on the samples at a voltage of 8 KV for 2 minutes. The current was kept constant at 5 mA during the sputter process.

Work conducted on the characterization of sensing films shows that drop casting particles (S1) (suspended in α-terpineol) is the best way to obtain uniform films. Fig 21 shows distribution of the particles (S1) over the sample for spin coating particles suspended in different ratios of Terpineol/ Ethanol. The different ratios for the mixture were (1/2 and 3/4 Terpineol/Ethanol) and (100% Terpineol). The SEM images show the formation of discontinuous film on the samples (S1). The size of the islands on the sample was observed to increase with the increasing ratio of Terpineol/Ethanol. The discontinuity in the film was attributed to the force on the particles during spin-coating. In order to confirm this, particles suspended in 100% α-terpineol were drop-casted – 16.3 mg/ml - over the samples and kept in the oven for 2 hrs at 80 ^{o}C to evaporate the terpineol. Platinum was then sputtered on the samples at a voltage of 8 KV for 2 minutes. The current was kept constant at 5 mA during the sputter process. The samples were investigated under the F-SEM for their continuity and uniformity. A continuous and uniform film was observed, as in Fig 22, for the sample with drop-casted particles suspended in 100 % α-terpineol.

Based on the morphology and uniformity study, particles suspended in α-terpineol were drop-cast in order to fabricate gas sensors for all the gas sensing measurements.

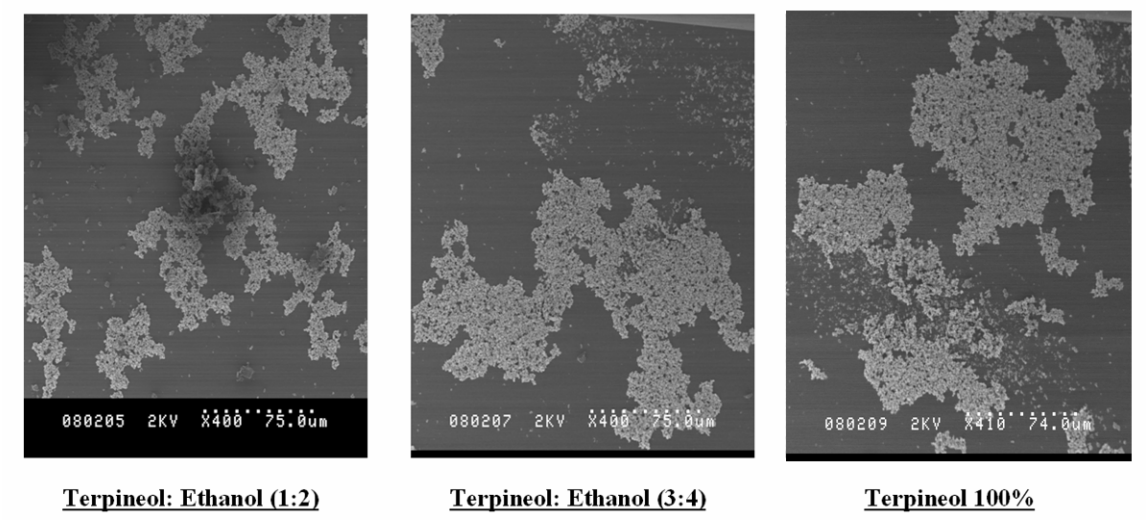

Fig 21: SEM images showing discontinuous films for spin coating ZnO nano-platelets

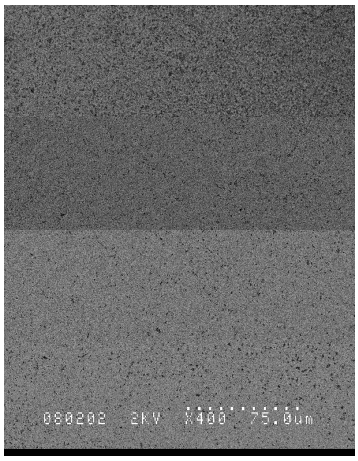

Fig 22: SEM image showing continuous film for drop casting ZnO nano-platelets.

The sensitivity of a material has a strong dependence on its surface area which in-turn depends on the size of the particles and the porosity of the material. Higher surface area could be obtained with smaller particle size and more porous material. Surface area for these particles was determined by Brunauer, Emmet and Teller (BET) Sorptometer. BET Sorptometer accurately measures total surface area, mean pore size, pore size

distribution, pore volume, and pore structure. The equilibrium volume of the gas adsorbed on a sample was determined by measuring the decrease in pressure for the known volume of N_2 gas at a controlled pressure and temperature (77K). This decrease in pressure was the result of the expansion of N_2 gas as it was released from the manifold to the sample cell and the adsorption of gas on to the sample. The pressure of N_2 was then increased close to the equilibrium vapor pressure which resulted in condensation of N_2 in pores. This pressure yields surface area and pore diameter for the samples. The surface area measurements were performed by our collaborators at Miami University of Ohio. The results obtained from BET measurements show a surface area of 10.5 m^2/g and 21.5 m^2/g for S1and S2 respectively.

As mentioned before, ZnO nano-materials when drop-casted over the sample resulted in the formation of uniform films. This technique was then used to fabricate gas sensors using both commercially bought and MEMS based platforms. Change in resistance of these nano-materials was then monitored for different gases and organic solvents. The following sections discuss the response of these resistive gas sensors to various analytes in detail.

3.2 Resistive Gas Sensors

3.2.1 Sensitivity to Hydrogen

Initial experiments were performed to ensure repeatability and reproducibility of the ZnO nano-platelets (S1) with H_2 gas. The sensor shows repeatable results for sensitivity towards H_2 with similar operating conditions for all experiments. Fig 25 shows

the response of the sample S1 drop casted on MSP–632 to 80 parts per million (PPM) of H_2 gas at room temperature for 2.5 SLM flow of carrier gas and a voltage bias of 5V across the inter-digitated electrodes. A voltage bias of 5V was chosen to maximize the signal to noise ratio as discussed. All the runs were conducted for the same input conditions in order to see the repeatability of the sensor to the analyte which was confirmed by the overlapped curves in Fig 23. N_2 was used as the carrier gas and air was used for recovering the sensor back to initial state.

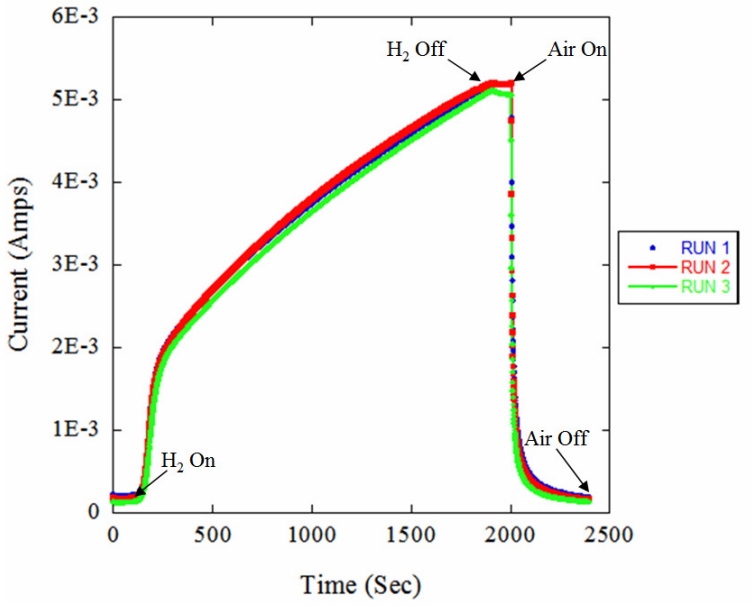

Fig 23: Response of ZnO nano-platelets to 80 PPM H2 at room temperature.

The sensor shows a large change in current initially after the introduction of the analyte after which the slope of the change seems to flatten out which was confirmed by calculation of the slope of the current in both the regions of operation. The change in current dropped from an initial value of 25µA/sec to 2.5µA/sec, likely due to an increase in occupancy of the reaction sites at the surface of the sensing film. This can be related to the Langmuir's theory for adsorbent isotherms.

The sensing mechanism for H_2 has been proposed to be based on the principle of change in surface conductivity with the introduction of the analyte in the system. The Pt catalyst results in the formation of highly reactive atomic hydrogen [47]. The atomic hydrogen readily oxidizes, resulting in the liberation of electrons at the surface and also leading to the formation of elemental zinc on the surface which causes the rise in current on exposure to H_2, as in Fig 25. The sensing mechanism of ZnO to H_2 can be seen in Eq 5 and 6 [28].

$$ZnO \leftrightarrow Zn^{+2} + O^{2-} \qquad \text{Eq 5.}$$

$$4H(Pt^{2+}) + O^{2-}_{(ads)} \leftrightarrow 2H_2O + e^{-} \qquad \text{Eq 6.}$$

Recovery of the system was observed only under flow of air (oxygen). This can be understood in light of Eq 5. Introduction of the O_2 in the system oxidizes the elemental zinc, thus resulting in an increase in resistance of the system with the formation of ZnO. However, Eq 6 suggests formation of water at the surface of the film, which may inhibit the oxidation of some elemental zinc and is believed to result in the incomplete recovery of the system as discussed below.

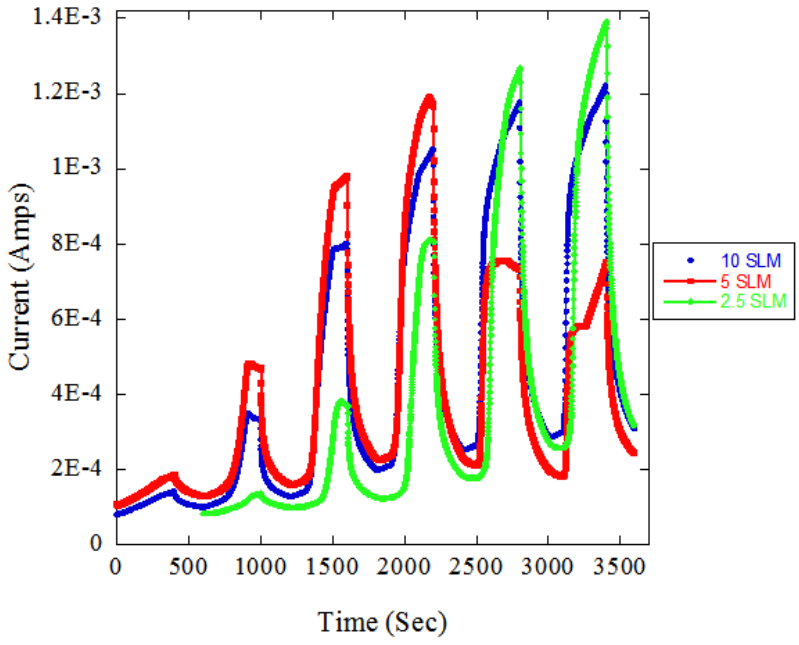

Fig 24: Response of ZnO nano-platelets to 20, 40, 60, 80, 159, 237 PPM H_2 at 25°C.

The repeatability of the sensor shown above confirms stability and reliability of the response of the sample (S1) to the analyte. In order to determine the lowest concentration that can be detected at room temperature sensitivity of the nano-platelets was measured for different concentrations of analyte at room temperature. Fig 24 shows the response to H_2 at different concentration (20, 40, 60, 80, 159, 237 PPM) at room temperature for various carrier gas flows (2.5, 5, 10 SLM). The sensor depicts incomplete recovery at room temperature, which is possibly due to the traces of elemental Zn in the material, which were not oxidized at the time of recovery owing to the formation of water at the surface (see Eq. 6). A similar trend was observed for the sensor with other carrier gas flows at room temperature. In order to confirm the cause for the incomplete recovery of the sensor, sensitivity of the nano-platelets was measured at 150°C – above the boiling point of water. Results suggest complete recovery of the sensor at this temperature, as in

Fig 25. Also, shorter response and recovery times were observed at high temperatures as an increase in the chemical kinetics at higher temperatures results in occupation of all the reaction sites in a duration of 200 seconds – reaction time for all the sensing measurements.

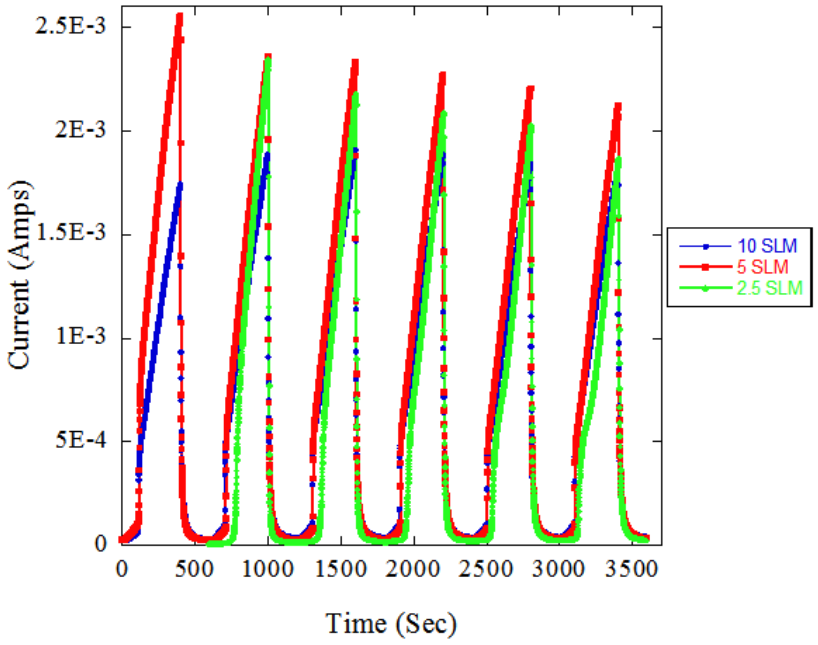

Fig 25: Response of ZnO nano-platelets to 20, 40, 60, 80, 159, 237 PPM H_2 at 150^{o}C.

The response and recovery time were also investigated as a function of the carrier gas flow in the system. The data suggests longer response and recovery time for a 2.5 SLM of carrier gas whereas shorter times were observed with the increase in carrier gas flow. This can be understood by Langmuir's equation (see Eq 7) which suggests that with the increase in carrier gas flow the pressure of the adsorbate on the sensing film increases which results in an increased number of atoms to be adsorbed at the surface thus resulting

in a better response in a duration of 200 seconds (reaction time for all the sensing measurements.) Langmuir's equation is given as:

$$\theta = \frac{\alpha \cdot P}{1 + \alpha \cdot P} \qquad \text{Eq 7.}$$

where θ is the percentage coverage of the surface, P is the gas pressure, and α is a constant and depends on operating temperature.

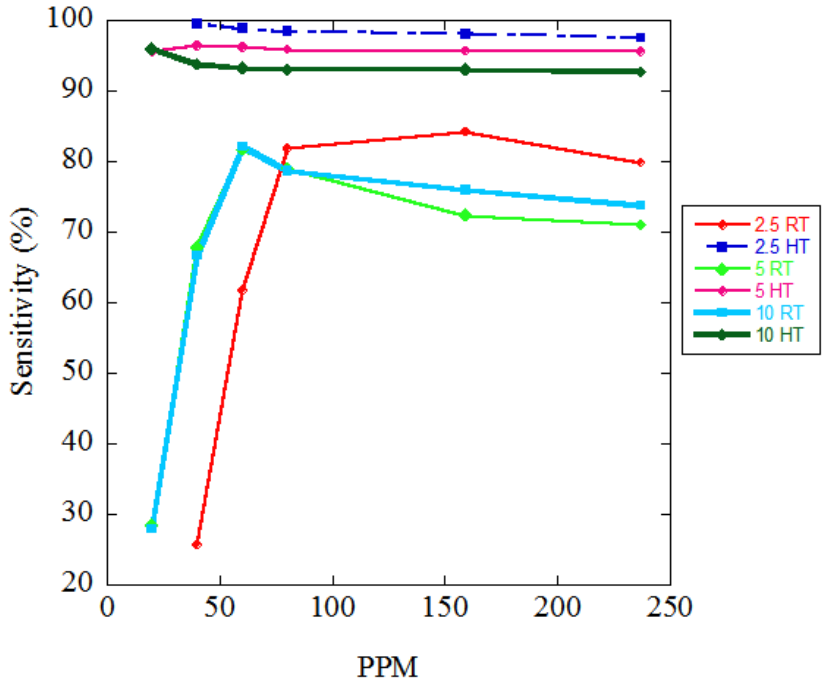

Fig 26: Sensitivity to different concentrations of H_2 at 25°C and 150°C for S1.

The expression used for the calculation of sensitivity in our experiments was derived from Eq 1 based on Ohm's law and is given by Eq 8.

$$S(\%) = \frac{I_{gas} - I_{air}}{I_{gas}} \times 100$$

Eq 8.

where I_{gas} is the current after exposure to gas and I_{air} is the initial current.

The sensitivity of the senor (S1) calculated from Eq 8 can be plotted for different concentrations of the analyte as in Fig 26. The response of the sensors saturates at higher concentrations of the analyte resulting in a maximum value of sensitivity which can be achieved. This can be understood by relation to the theory of adsorbtion isotherms by Irving Langmuir. The theory is based on four basic assumptions which can be listed as follows [24].

1. All the adsorption sites are equal.
2. Adsorbed molecules do not interact.
3. All adsorption occurs through the same mechanism.
4. At the maximum adsorption, only a monolayer is formed: i.e. the molecules of the analyte do not adsorb on each other but only on the molecules of the sensing film.

The above assumptions suggest that the sensitivity of the sensor would increase with the increase in concentration of the analyte till a monolayer of the adsorbate is formed on the surface of the adsorbent, after which the response seems to saturate because of the unavailability of reaction sites. In order to confirm the fore stated assumptions, Langmuir's equation given in Eq. 7 was plotted for different values of pressure and a fixed alpha. The percent coverage area obtained was then plotted for these values of pressure. The pressure of the analyte in the sensing chamber varies with the concentration

and the sensitivity is correlated to the percent coverage area of the sensing film. Fig 27 shows an overlay plot of recorded sensitivity with the values of θ obtained from Langmuir's equation. Similar functional form was observed for both the recorded and theoretical sensitivity values. The linear and saturation regions are demarcated in the figure for the convenience of the reader.

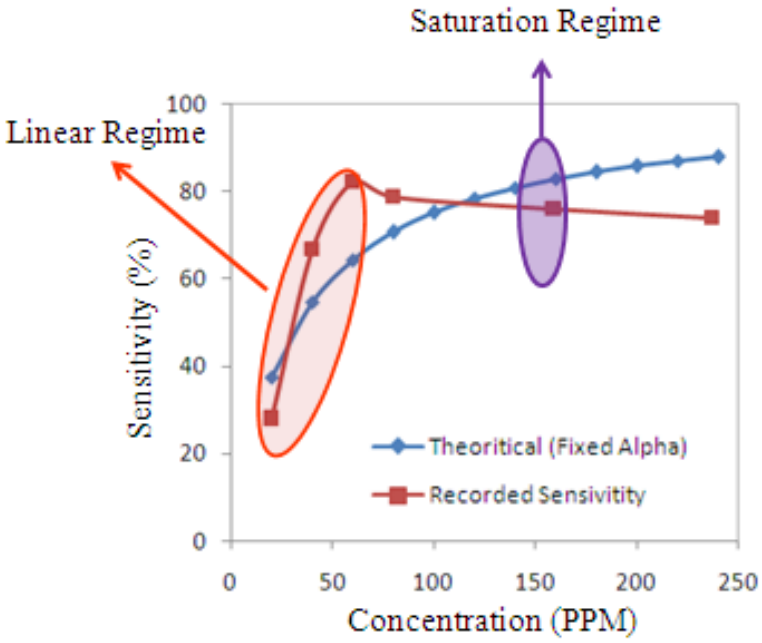

Fig 27: Overlay plot of recorded and theoretical sensitivity values.

Fig 26 shows a rise in the sensitivity of (S1) with increasing concentration till the saturation limit at room temperature, after which the unavailability of reaction sites on the surface of the adsorbent limit the sensitivity of the senor, which confirms the above discussion. However, an increase in the chemical kinetics at higher temperatures results in occupation of all the reaction sites in a duration of 200 seconds – reaction time for all the sensing measurements – which causes the sensor to saturate even at lower concentrations of the analyte as in Fig 26. Data suggests that at higher temperatures even

lower concentrations of H_2 can be detected; however due to the incapability of the system at present to flow small traces of H_2 in the PPB range, this was not confirmed experimentally. Sensitivities near 96% for 20 ppm H_2 gas were observed at 150°C as compared to that of 28% for 20 PPM of H_2 at room temperature. Measurements at temperatures higher than 150°C were not recorded as the sensitivity of the sensor was almost 100% at around 150°C.

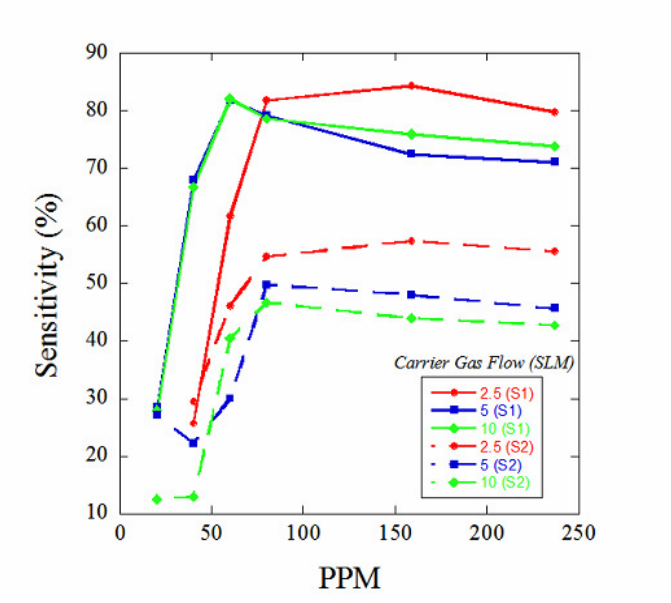

Fig 28: Sensitivity (S1 v/s S2 at 25°C)

In order to estimate the effect of material properties like surface area and porosity, gas sensing measurements were repeated for sample S2. Response of sample S2 to H_2 at different concentration (20, 40, 60, 80, 159, 237 PPM) was measured at room temperature and higher temperatures for various carrier gas flows (2.5, 5, 10 SLM). Fig 28 compares the response of S1 and S2 to H_2 gas at room temperature. Similar effects like

saturation at higher concentration of the analyte and incomplete recovery at room temperature were observed.

The behavior for saturation at higher concentration for sample S2 was because of the occupancy of reaction sites given by Langmuir's theory of isotherms as discussed before. Also the incomplete recovery was attributed to the formation of water at the surface of the sensing film. However higher sensitivity was observed for sample S1 as in Fig 28. Higher sensitivity of S1 can be explained by the lower packing density for the larger particles for the same weight % ratio. A lower packing density for the sample S1 would thus increase the porosity of the material in-turn increasing the surface area for gas sensing.

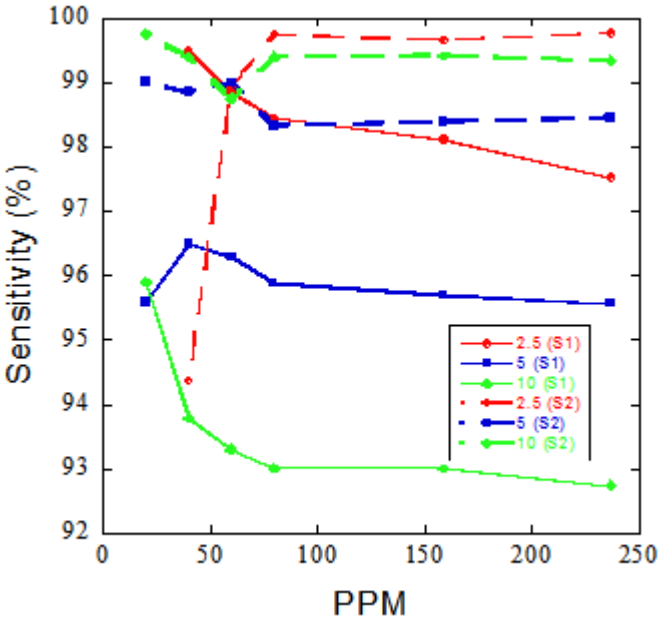

Fig 29: Sensitivity (S1 v/s S2 at 150^{o}C)

Fig 29 shows sensitivity of the samples S1 and S2 to H_2 gas at 150^{o}C. Both samples S1 and S2 show sensitivities in the same range, for measurements with H_2 at

higher temperatures (150^{o}C). This is because of the increase in chemical kinetics at higher temperatures as discussed in the previous sections. As evident from the graphs, for each sample, lower carrier gas flows resulted in higher sensitivities because the reduced flow of gas in the chamber allows more time for the reaction between the analyte and sensing film.

Highly sensitive sensors operating at room temperature were successfully fabricated and tested for H_2 gas. The series of experiments conducted, successfully showed effect of carrier gas velocity, concentration and operating temperature on response and recovery of the sensor. Also, higher response was seen for sample S1 when compared to S2. Based on higher sensitivity values observed for sample S1, all further experimentation with ZnO was carried out using ZnO nano-platelets. Further research was also done in order to understand the catalytic effect of platinum on sensitivity to H_2 gas. The following section discusses these results and others obtained with S1 for different analytes.

3.2.2 Response to Other Gases and Organic Solvents

The effect of the Pt catalyst on H_2 gas sensing was confirmed for both room temperature and high temperature measurements using the in-house fabricated MEMS gas sensors. Fig 30 shows the response of S1 to H_2 gas at 150^{o}C with Pt and Cu as the electrode metals. Copper was chosen as the other electrode metal as it does not act as a catalyst for sensing H_2 gas. A comparison of sensitivity values observed with both Pt and Cu based electrodes confirm the catalytic effect of Pt. The conductance of the ZnO film increases on introducing CO (reducing gas) [14]. This can be depicted by Eq 9 which

shows the formation of two electrons on reaction of CO with the adsorbed oxygen gas at the surface of the sensing film. Both the elemental Zn and the electrons formed as a result of this reaction contribute to the increase in current on exposure to CO.

$$2CO + O^{2-}(ads) = 2CO_2 + 2e^- \qquad \text{Eq 9.}$$

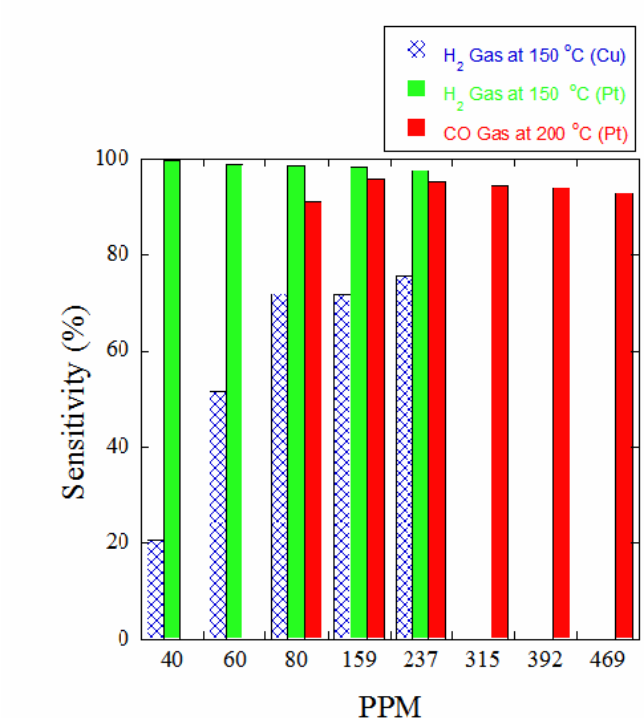

Fig 30: Response of S1 to CO and H_2 with Pt & Cu electrodes.

Significantly lower sensitivity was observed for the Cu electrodes, confirming the catalytic effect of Pt. Also, no response was observed at room temperature for S1 with Cu electrodes. Additionally, the sensitivity of S1 to various concentrations of CO (80, 159, 237, 315, 392 and 469 PPM), at operating temperatures of 200^{o}C was recorded (see Fig 31). Values near 90% for 80 PPM CO were recorded at 200^{o}C.

Sensitivity results of the nano-platelets were also recorded for different analytes. Initial set of measurements were carried out at room temperature and showed almost no response of the nano-platelets to any gases or organic solvents. Thus an operating temperature of 200^{o}C was chosen for all further experiments. Results to various gases and organic solvents are presented in the following figures.

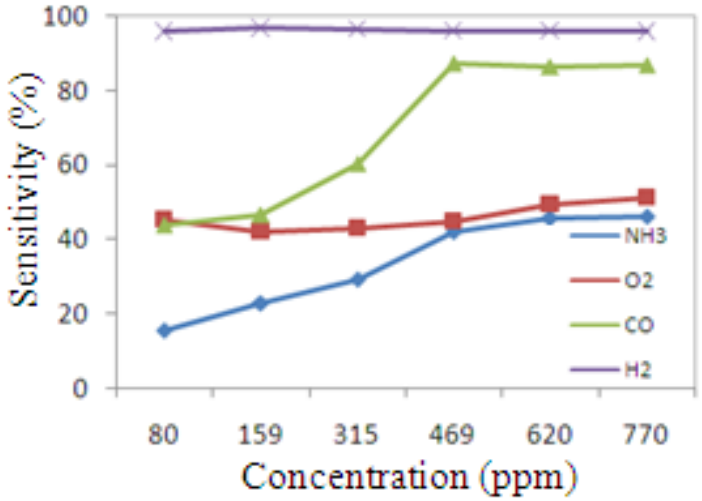

Fig 31: Response of ZnO nano-platelets to various gaseous analytes

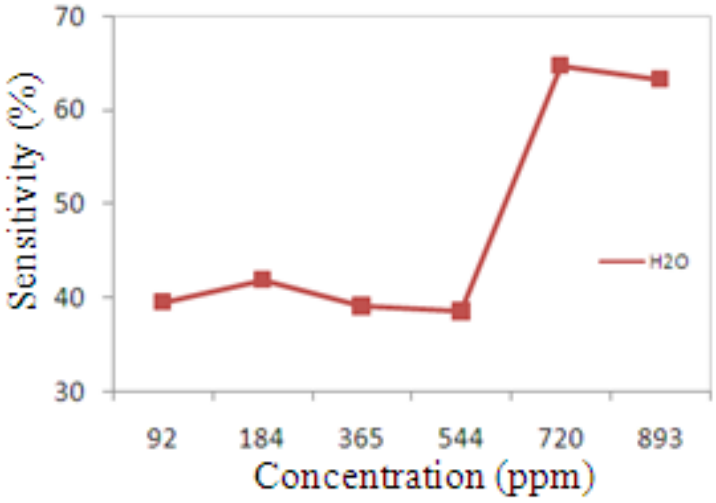

Fig 32: Response of ZnO nano-platelets to H_2O

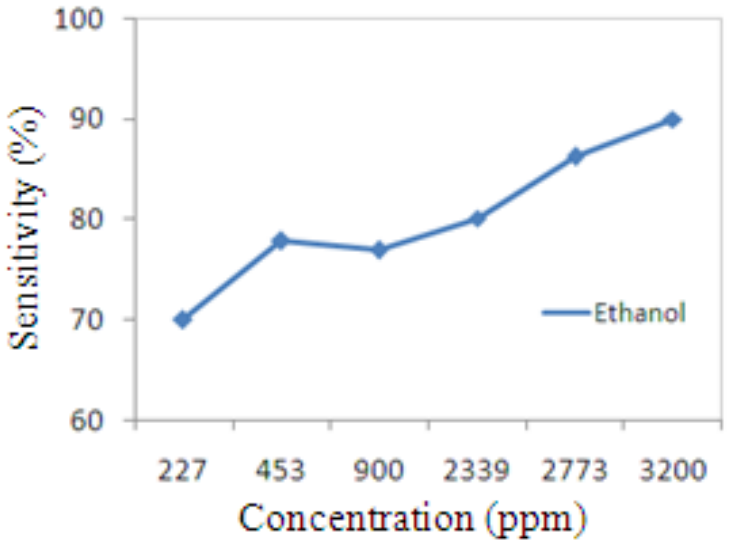

Fig 33: Response of ZnO nano-platelets to C_2H_5OH

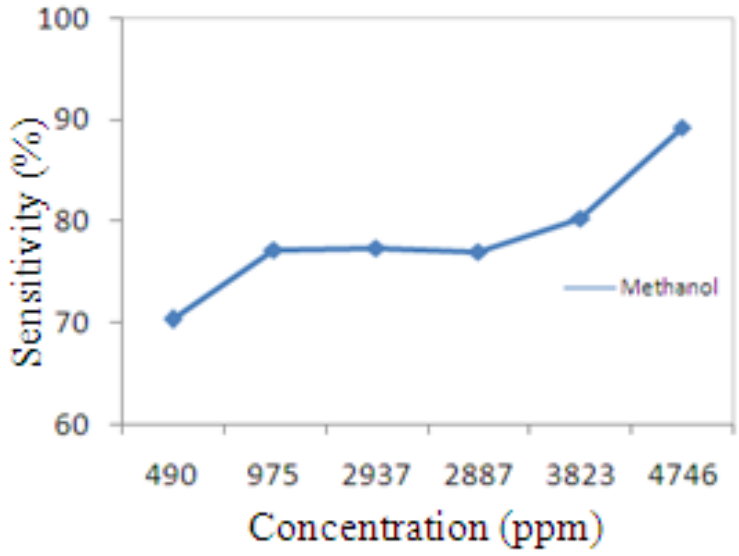

Fig 34: Response of ZnO nano-platelets to CH_3OH

Maximum response was recorded for H_2 at 200^oC. This was because of the presence of Pt electrodes- which acts as a catalyst- and high temperature – which increases the chemical kinetics of the reaction. When compared to H_2, lower response

was observed for CO, O_2 and NH_3 at the given operating conditions. Sensitivity on the order of 60% was observed at 315 PPM CO as compared to values of sensitivity about 42% for O_2 and 29% for NH_3.

Different values of sensitivity were observed for various concentration of different analytes. The difference in concentration of the different analytes for the same flow is because of the difference in vapor pressure at a given temperature and pressure. Lower concentration of the solvents is owing to the lower vapor pressure for the same flow of N_2 through the system.

Sensitivity to different solvents cannot be directly compared using the above data as all the solvents do not have the same concentrations owing to different vapor pressures at room temperature. However this can either be done by varying the temperature in order to measure the sensitivity of the ZnO to these analytes at a constant value of concentration or comparing sensitivities at some specific concentration common to all or most of the solvents. This can be seen in Table 10 where the sensitivity of the nano-platelets is compared to the approximately equal concentrations of the solvents.

Solvent	Concentration (PPM)	Sensitivity %
C_2H_5OH	453	77.76
CH_3OH	490	70.26
H_2O	544	38.43

Table 10. Comparison of sensitivity of ZnO nano-platelets to different solvents.

Data suggests that the nano-platelets show better sensitivity towards C_2H_5OH when compared to CH_3OH and H_2O for about the same concentration. The sensing

mechanism of Ethanol with ZnO is explained by Chen et al [30] and is summarized in Eq 10.

$$CH_3CH_2OH_{ads} + 6O_{ads}^{-} \rightarrow 2CO_2 + 3H_2O + 6e^{-} \qquad \text{Eq 10}$$

As shown in Eq 10, the analyte (ethanol) reduces the sensing material (ZnO) by reacting with the adsorbed oxygen, thus leading to the formation of free electrons on the surface. As mentioned before for H_2, both elemental Zn and free electrons contribute to the increase in current.

Sensitivity of ZnO to various gases and organic solvents was successfully recorded. However, the higher operating temperatures required for the reaction may limit the integration of these nano-particles in low power micro-machined sensors. Sensitivity to various gases and organic solvents was also demonstrated with Arc produced tubes and HiPCo produced SWCNTs, where promising results were observed for HiPCo tubes at room temperature. These results are discussed in Chapter IV.

Based on the theory of adsorbtion isotherms by Irving Langmuir as discussed above, the number of available reaction sites affects the sensitivity of the sensor. Also the number of reaction sites is dependent on the surface area of the adsorbent. This implies that an increase or decrease in the surface area would directly affect the sensitivity of the sensor. In order to study this sensitivity results for MEMS based gas sensors were recorded for varying device and process parameters. The following section discusses these results in detail.

3.3 Design of Experiment Study

Initially, gas sensing measurements were recorded for only 40 and 80 PPM H_2 gas at room temperature, using MEMS sensor platforms fabricated using sample S1. Standard experimentation procedure was carried out for H_2 gas at room temperature as discussed in the previous chapters for ZnO nano-platelets. The results obtained, were used as the basis for the in-depth design of experiments study.

Initial results with the MEMS based sensors show the effect of device parameters on gas sensitivity. As expected, higher sensitivity values were recorded for devices with more inter-digitated electrodes for both 40 and 80 PPM of analyte exposures. This is due to the increase in surface area with the increasing number of electrodes. Also addition of resistance in parallel reduces the overall resistance of the system thus increasing the current in the system. It can be seen from Fig 35 that increasing the number of fingers increases the gas sensitivity drastically.

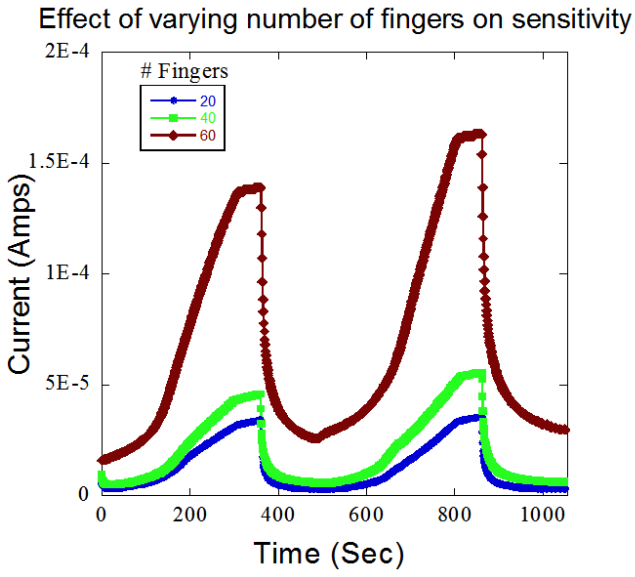

Fig 35: Effect of # of fingers on gas sensitivity.

In addition to the efforts made to understand the effect of number of electrodes on sensitivity of the sensor, experiments were also performed to record effect of reduced spacing between the inter-digitated electrodes on gas sensitivity. Fig 36 depicts that reduction in the spacing between the electrodes increased the response of the sensor. This is because for a reduced spacing between the electrodes, the electrons donated at the surface would have to travel a shorter distance before being collected by the electrodes. Thus an increase in current will be observed in a shorter time for lesser spacing. This effect should be more prominent in highly resistive films like ZnO. The sensors with lesser spacing also show a shorter recovery time when exposed to air.

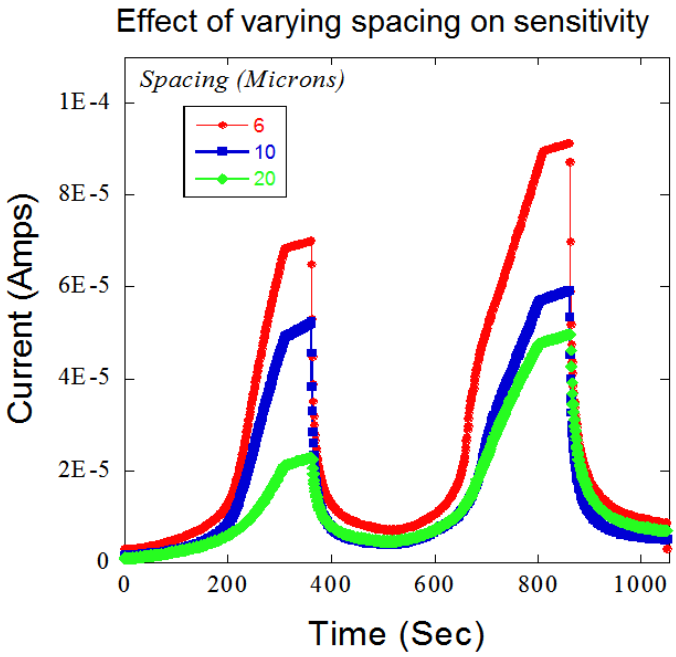

Fig 36: Effect of spacing on gas sensitivity

Based on these initial results, an in-depth study was performed to understand the effect of device parameters on gas sensitivity. As mentioned before, initially, the device parameters considered for the experiments were spacing between the electrodes and the number of electrodes. Whereas, voltage bias across the electrodes, concentration of the analyte and the operating temperature were the process parameters for the experiments. The details of the experiments and results are discussed in the subsequent sections.

3.3.1 Effect of Varying Electrode Spacing

As mentioned above, both device and process parameters were varied in order to model the sensitivity of the sensor. These factors and their range of operation are tabulated in Table 7 in Chapter 2. The results obtained for varying spacing of the IDEs are discussed in this section.

Three levels of variation were considered for all the parameters except for concentration of the analyte, which was varied in five different levels. All the parameters were varied from the lower limit to the upper limit in regular intervals. A total of 47 data points were collected in order to analyze the effect of each device parameter on sensitivity. Statistical software JMP was used to analyze this response and summarize the results. Fig 37 shows the JMP results of the effect of spacing on gas sensitivity for the foresaid parameters.

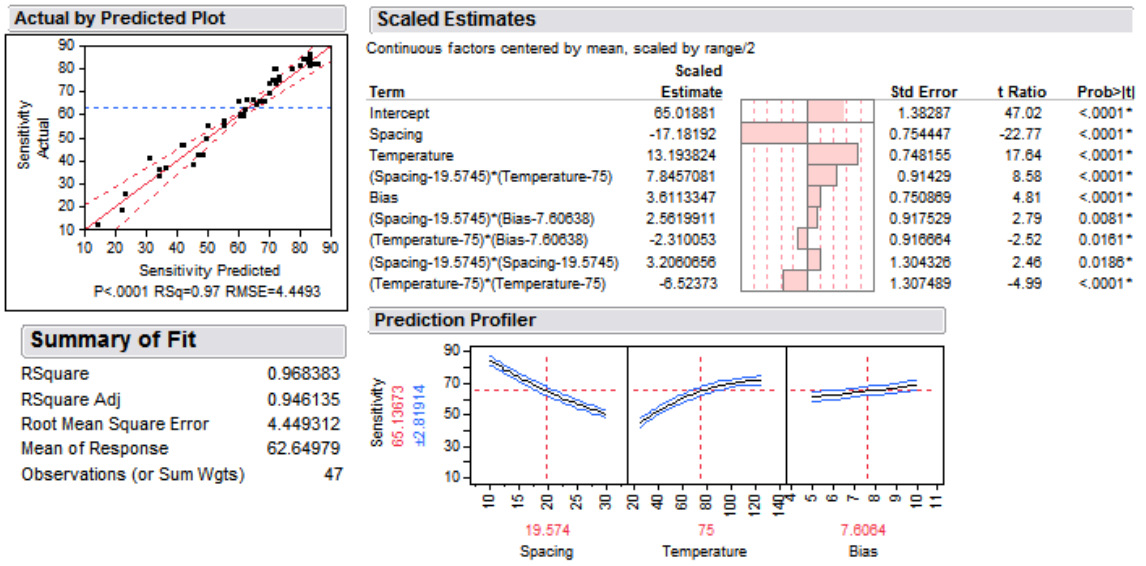

Fig 37: DOE results for effect of spacing on gas sensitivity (Initial Results).

Data suggests normal distribution of the data points. Spacing, Operating temperature and Bias were the first order effects, which were identified to have a sizable effect on gas sensitivity. The coefficient of Spacing in the model was negative, meaning that a decreasing spacing would result in more sensitivity. Also, the model depicts a large huge effect on sensitivity with increasing temperature and mild but positive effect of voltage bias on sensitivity. It is also evident that increasing temperature further drives the sensor into saturation for the given concentration range. These results are along the same lines of the initial results in Fig 36 with the MEMS sensors.

However, it is to be noted that the model depicts that the concentration of the analyte does not have a significant impact on the gas sensitivity. In other words, sensitivity of the sensor was independent of the concentration of the analyte. This not only contradicts the initial set of results but also violates the Langmuir's theory of adsorption isotherms. This is can be understood as follows. Due to the highly sensitive

nature of ZnO nano-platelets in the presence of Pt catalyst and high operating temperatures (75°C and 150°C) the sensor always operates in the saturation regime of operation. Thus, maximum sensitivity values were recorded for the whole range of concentration (20, 30, 40, 50 and 60 PPM). This suggests that for the given temperature conditions, the chosen concentration settings were too high for the sensor to operate in the linear region of operation.

The results obtained with these DOE runs were promising as a negative dependence of sensitivity was seen with spacing between the electrodes. Also the voltage bias shows consistent slope with both the experiments. However, as effect of temperature reduces the impact of the concentration of the analyte on gas sensitivity, these set of experiments were repeated at room temperature. These factors were tabulated in Table 8 in the previous chapters. The range of operation for the variables but temperature was chosen to be the same as before, with the temperature constant at 25°C. Fig 38 shows the JMP results of these revised efforts.

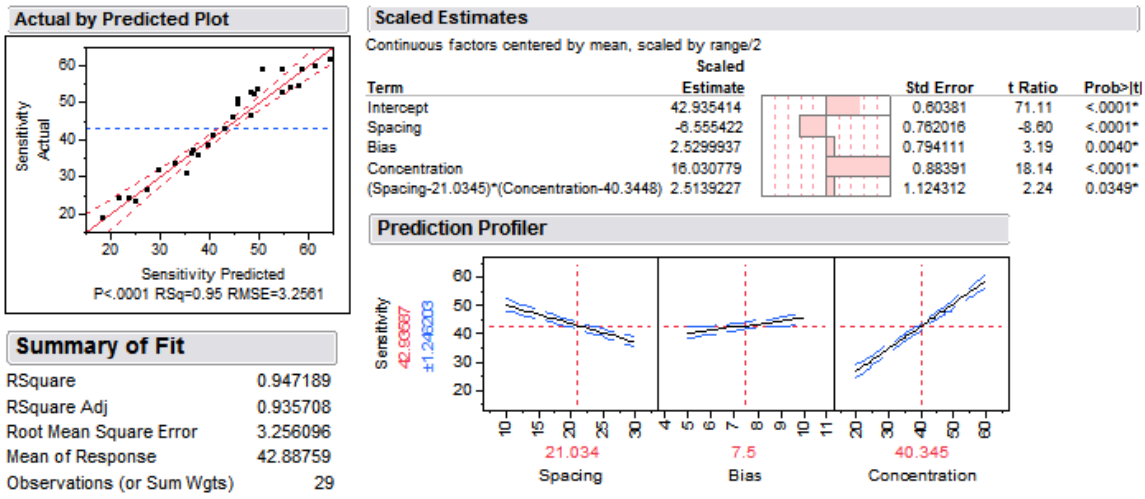

Fig 38: DOE results for effect of spacing on gas sensitivity (Final Results).

Looking closely at Fig 38, the Prediction Profiler shows increase in sensitivity for reducing spacing between the inter-digitated electrodes. This is as the electrons have to travel a shorter distance before they get collected by the electrodes. This phenomenon may not be of much significance while dealing with very conductive sensing films; however with ZnO this significantly affects the sensitivity and the response time of the gas sensor. Fig 39 shows the effect of increasing spacing on gas sensitivity. Results in Fig 39 were plotted for only 5V bias across the IDEs.

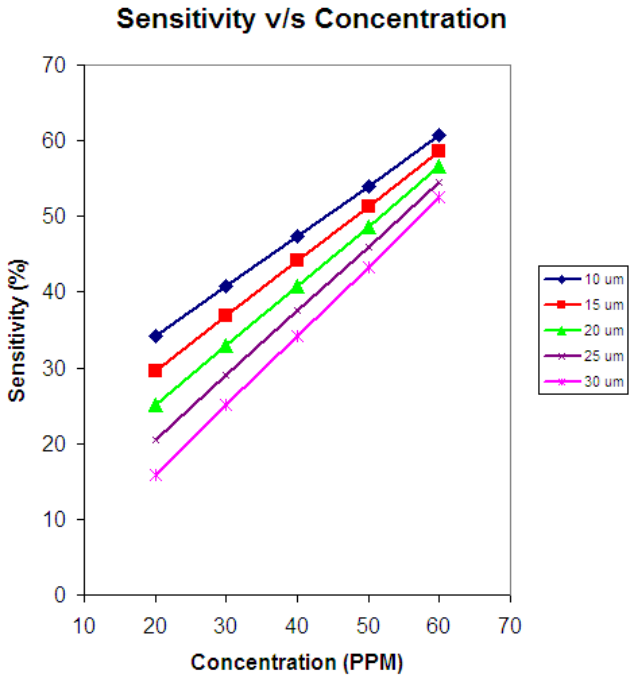

Fig 39: Effect of increasing spacing on gas sensitivity

Data in Fig 39 suggests lower sensitivity values observed for increasing spacing. Also it can be seen that the effect of bias is maximum for lower concentration values of the analyte and the difference in sensitivity values reduces with increasing spacing. This may be because of the limited number of electrons available at lower concentrations of

the analyte which contribute to the sensitivity of the sensor. Also, bias seems to show a positive effect on the gas sensitivity. This can be looked at as keeping the electric field constant between the electrodes by increasing the voltage bias with increased spacing. Fig 40 shows the sensitivity of increasing bias on gas sensitivity. Results in Fig 40 were plotted only for sensor head with 10 micron spacing.

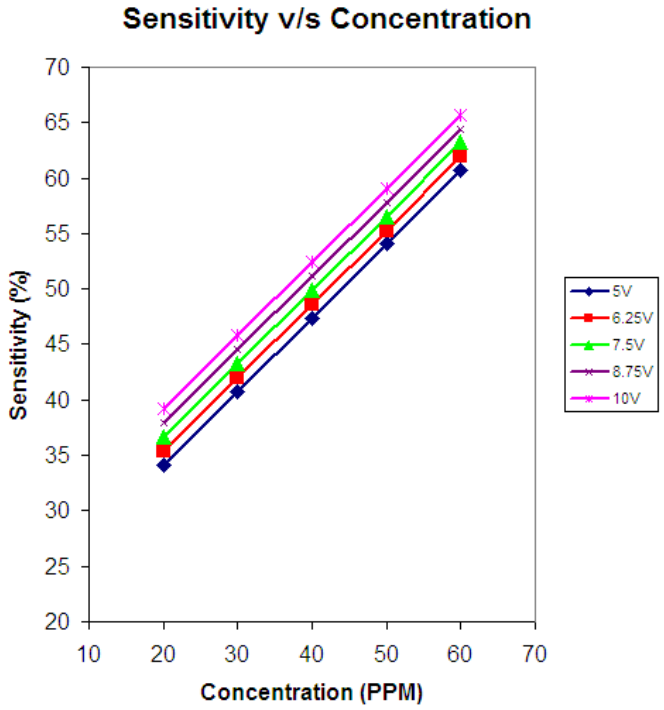

Fig 40: Effect of increasing Bias on gas sensitivity

As evident from the prediction profiler in Fig 38 and Fig 40, the sensor operates in the linear region of the operation for the given range of concentration. This is in conjunction with previous results observed with the commercial sensor head and in Fig 26. The sensor head MSP-632 operates in the linear region of operation up-to 60 PPM after which the sensitivity saturates as the concentration is increased to 80PPM. Other

factors effecting the boundaries of linear and saturation regions of the sensor would be the amount of material used for sensor fabrication and the form the nano-particles take, after the sensor is subjected to the heat treatment in order to dry off the solvent. Also, the values of sensitivity achieved with MEMs fabricated sensor as in Fig 40 was up to 60% for 60PPM H_2 gas and a bias of 5V across the electrodes, when compared to that of 81.7% for MSP-632 for the same concentration of the analyte. This was hypothesized to be because of higher surface area for the MSP-632 which had 50 pairs of inter-digitated electrodes when compared to 20 pair for the MEMs sensor.

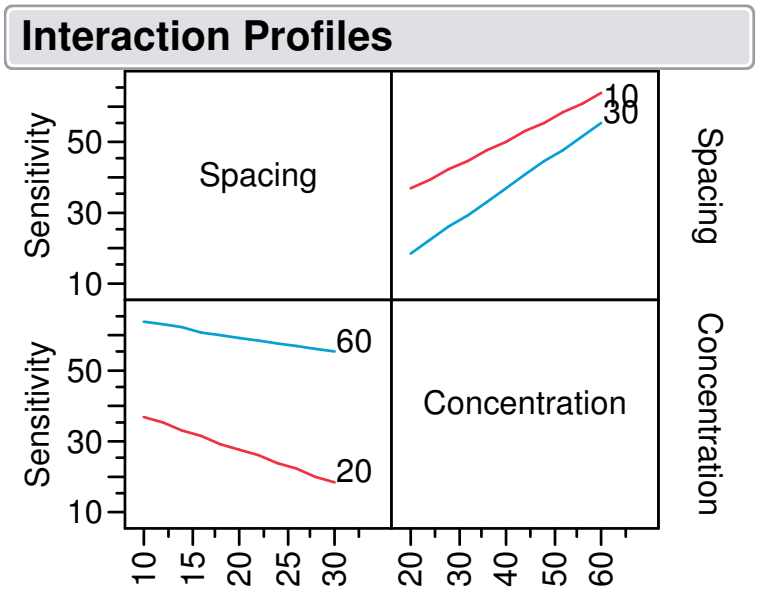

Fig 41: Interaction effects between Spacing and Concentration

Interaction effects were observed between spacing of the IDEs and concentration of the analyte. This is shown by the non-parallel lines in Fig 41. As discussed earlier and as shown in Fig 41, significant difference in sensitivity was observed at lower

concentrations of the analyte and this difference reduced with the increase in concentration. Based on the discussions above for the spacing study, sensitivity was modeled as in Eq 11. The sensitivity can be predicted for given conditions by replacing the variables in Eq 11 by design units.

$$Sensitivity = 42.93 - 6.55(Spacing) + 2.52(Bias) + 16.03(Conc) + 2.51(Spacing)(Conc) \quad \text{Eq 11}$$

Impressive results were observed for the measurements performed at room temperature. Higher values of sensitivity were observed with decreasing spacing as expected. Also, the higher effect of spacing on gas sensitivity was observed for lower values of concentration. Though the obtained results were highly dependent on the range of operation chosen for the process parameters, they were representative of previously observed results with the nano-platelets. Further experimentation was also carried out to understand the effect of increasing number of IDEs on gas sensitivity. These details are discussed in the following section.

3.3.2 Effect of Increase in Electrodes

Designed experiments were performed in order to understand the effect on increasing IDEs on sensitivity. These factors and their range of operation are tabulated in Table 7 in the previous chapters. As mentioned before, three levels of variation were considered for all the parameters except for concentration of the analyte, which was varied in five different levels. Fig 42 shows the JMP results of the effect of increasing IDEs on gas sensitivity.

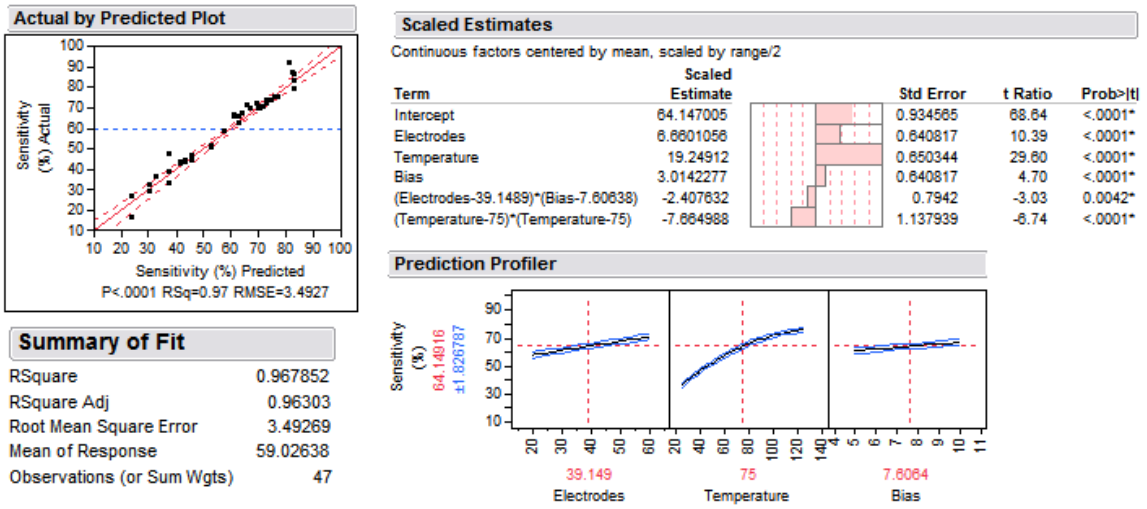

Fig 42: DOE results for effect of # of electrodes on gas sensitivity (Initial Results).

Fig 42 represents JMP results of the effect of number of electrodes on gas sensitivity. As observed for varying spacing study, temperature shows high impact on sensitivity with the sensor seems to saturate with increasing temperature and the voltage bias shows consistent slope for both the spacing and the electrode variation. The sensitivity was also observed to increase with the increasing number of electrodes. As discussed before, the sensitivity on the sensor was independent of the concentration of the analyte for the given range of temperature. Thus, another set of experiments were repeated at room temperature for varying electrode study. JMP results for varying the electrodes are represented in Fig 43 and discussed in the subsequent paragraphs.

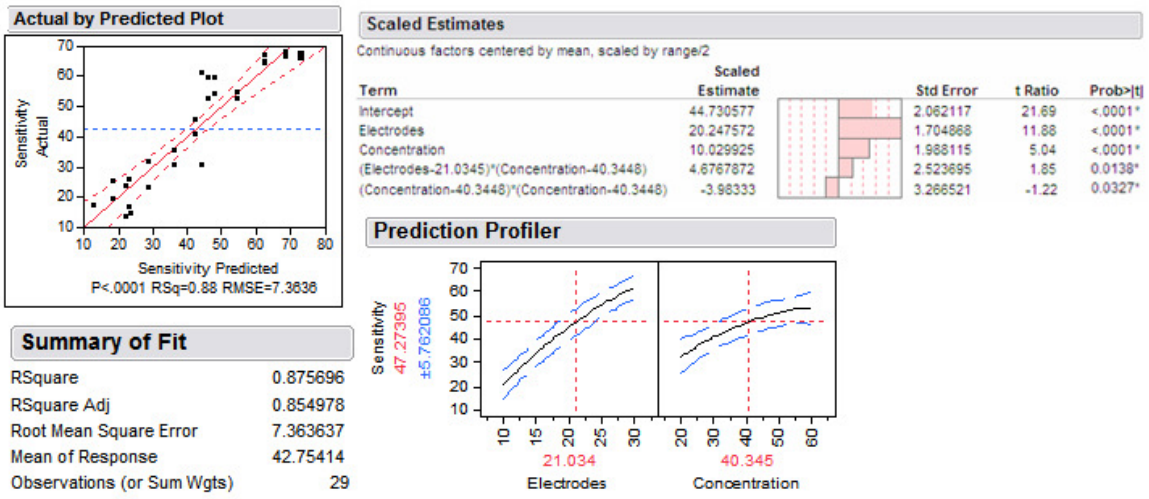

Fig 43: DOE results for effect of # of electrodes on gas sensitivity (Final Results).

Fig 43 shows results for sensitivity obtained with varying the number of electrodes for 20 micron spacing across the IDEs. The sensitivity of the sensor was recorded to increase with the increase in the number of electrodes. This was because of the increase in surface area with the increase in the number of electrodes. Fig 43 also shows only Electrodes and Concentration to be the significant factors affecting the sensitivity whereas; bias was identified as a non-significant factor. As all the measurements were taken with sensors having a constant spacing of 20 microns between the IDEs, applied voltage bias was not identified as a significant factor for sensitivity.

The sensitivity is also seen to saturate with increase in concentration in Fig 43. The fact that this effect was seen for the sensors with constant spacing and not with varying spacing can be explained by the possible variation in surface area that can result with similar gas sensor fabrication techniques.

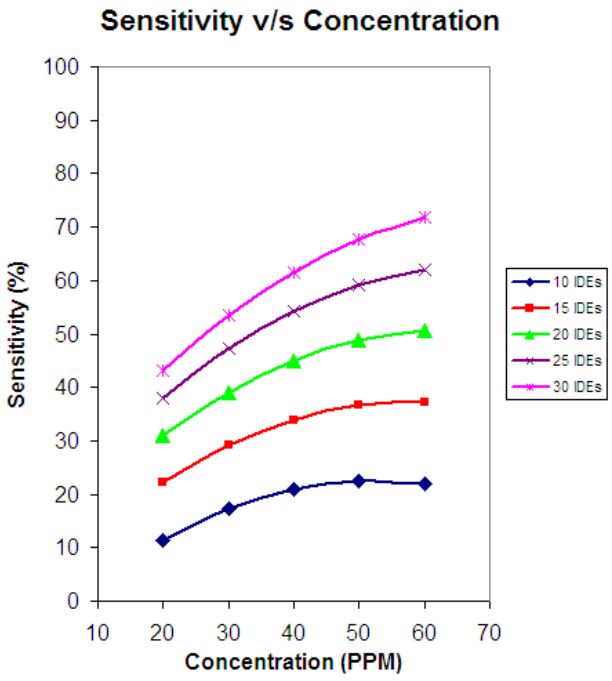

Fig 44: Effect of increasing IDEs on gas sensitivity

Fig 44 shows the effect of increasing IDEs on gas sensitivity with a constant voltage bias of 5V. As mentioned before, saturation of the sensitivity was observed for higher values of concentration. Also, higher values of sensitivity were achieved with 30 pair of IDEs when compared to 10 pairs. A quick comparison of Fig 44 with Fig 39 shows higher sensitivity values achieved for the same range of concentration with 30 IDEs -about 70% for 60 PPM – when compared to values on the order of 60% for 60 PPM with 20 IDEs.

Interaction effects between concentration and the number of IDEs can be seen in Fig 44. The sensitivity of the sensor is most affected at higher values of concentration. As discussed earlier, available reaction sites are directly proportional to the surface area of the sensing film. Hence, at higher concentrations the analyte molecules do not have

enough reaction sites available. This is also evident from Fig 45 where the difference in sensitivity for the number of IDEs increases with the increase in concentration.

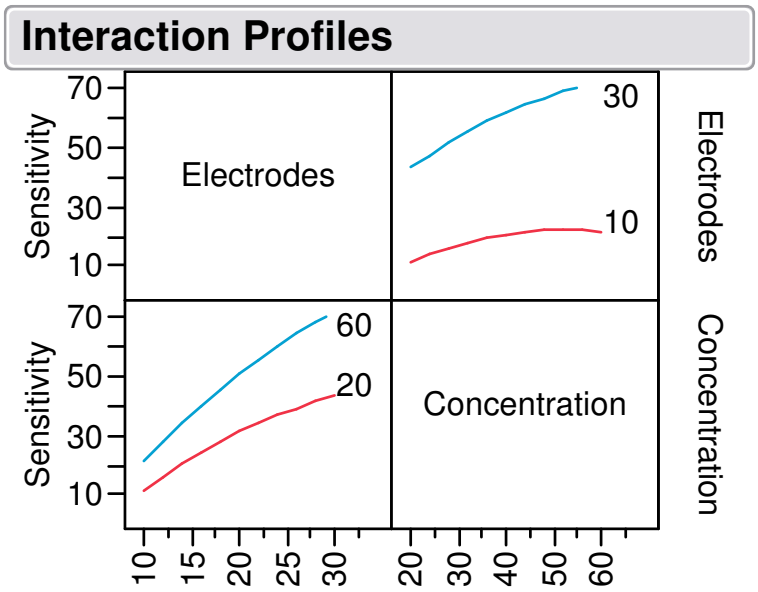

Fig 45: Interaction effects between Electrodes and Concentration.

Interaction effects between number of the IDEs and concentration of the analyte are shows by the non-parallel lines in Fig 43. As discussed earlier and as shown in Fig 44, sensitivity is impacted more at higher concentration for less number of IDEs due to the limited number reaction sites. Based on the discussions above for the varying IDEs study, sensitivity was modeled as in Eq 12. The sensitivity can be predicted for given conditions by replacing the variables in Eq 12 by design units.

$$Sensitivity = 44.73 + 20.24(IDEs) + 10.02(Conc) + 4.67(IDEs)(Conc) - 3.98(Conc)(Conc) \quad \text{Eq 12}$$

The sensitivity was successfully modeled for both varying spacing and varying electrodes studies. Also, the interaction effects between different parameters give an in-depth understanding of the sensing mechanism based on Langmuir's theory of adsorption isotherms. Sensitivity of ZnO was successfully recorded to various gases and organic solvents. However, these results were obtained only for higher operating temperatures which limit the integration of these nano-particles in micro-machined sensors. In order to sense various analytes at room temperature, carbon nano-tubes were used as the next step in the research. The following chapter discusses results obtained with CNT based sensors.

CHAPTER IV

Carbon Nanotubes Based Gas Sensors

4.1 Material Synthesis and Characterization

As discussed in the earlier chapters, carbon nanotubes were used for sensor fabrication due to the inability of ZnO based sensors to detect different gases and organic solvents at room temperature. Carbon nano-tubes based samples, namely Arc produced carbon nano-tubes and HiPCo produced SWCNTs (both commercially bought from Carbon Solutions inc.) were analyzed for this study. Several techniques have been developed to synthesize carbon nanotubes [53]; these include Arc Discharge, Laser Ablation and Chemical Vapor Deposition (CVD). Following sections discuss these synthesis techniques, material characterization and sensor fabrication details for these samples.

Arc Discharge tubes are produced by introducing an arc discharge across graphite electrodes. The yield for CNTs produced with this method is 30% by weight with the rest of the sample being carbon soot or ash. The sample contains a mixture of both single and multi walled tubes. The average length of these tubes is up to 50 microns [54].

Laser ablation tubes on the other hand are produced by vaporizing a graphite target with a pulsed laser in the presence of an inert gas in the chamber [53]. The yield of this method is about 70 % by weight and primarily produces single walled CNTs. Also

the diameter of the tubes produced can be controlled as a function of the reaction temperature [51].

CVD technique involves growth of carbon nanotubes on patterned metal nano-particles at high temperatures on the order of 700^{o}C. Most commonly used metals used are nickel, cobalt or iron. Growth is initiated by introducing a carbon containing gas (acetylene, ethanol or methane) in addition to a process gas (nitrogen or hydrogen). The carbon containing gas breaks up at the surface of the metal catalysts and nanotubes are formed at the edges of the nano-particles. CNTs produced with this method are a mixture of single walled and multi walled tubes with a yield varying from 20% to nearly 100% [48].

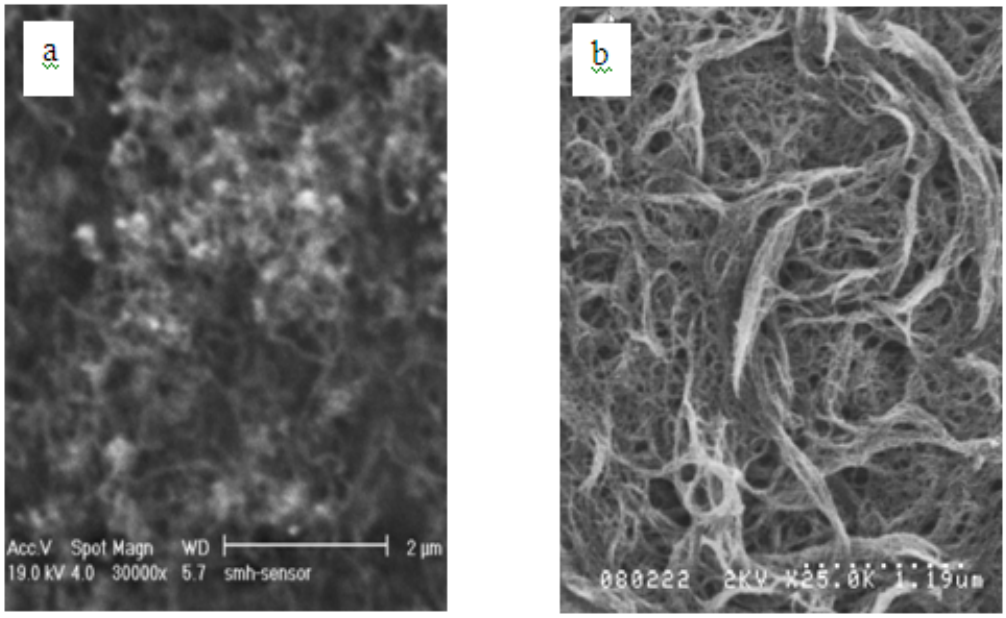

Fig 46: SEM Images of a) Arc Produced Carbon Nano-Tubes b) HiPCo SWCNTs

Samples of carbon nano-tubes based nano-materials used to fabricate gas sensors at R.I.T were commercially bought arc produced carbon nanotubes from Carbon Solutions inc. and Single Walled Carbon Nanotubes (SWCNTs) produced by HiPCo process as shown in Fig 46. SEM images demonstrate that SWCNTs produced using HiPCo process have more percentage of the carbon nano-tubes. The purity assessment on the Arc produced tubes was performed using UV-vis at the Nanopower Research Labs, suggests presence of 18% CNTs with amorphous carbon and other metal impurities. The UV-vis technique is used to see the absorbance of the CNTs for different wavelengths of light in order to assess their purity [55]. For the experiment performed at Nanopower Research Labs arc tubes were suspended in 2% weight/volume sodium cholate in water and were horn sonicated for 1/2 hour. Figure 47 shows a plot of absorbance v/s energy (ev) for same. Better peaks for absorbance are observed for more pure samples.

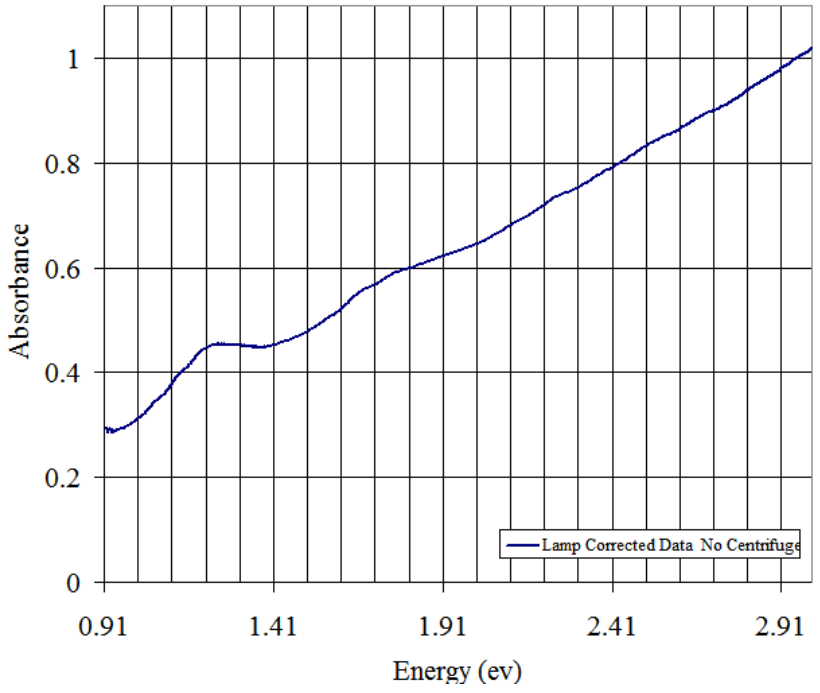

Fig 47. UV-vis measurement for assessment of CNTs.

Gas sensors using carbon nanotubes were successfully fabricated and tested, by measuring change in both resistance and impedance for arc produced tubes and HiPCo produced tubes respectively. For resistive gas sensors, a very small amount of tubes were dropcasted over commercial sensor platforms whereas for impedance spectroscopy based gas sensor, HiPCo tubes were screen printed on the cleaved MEMS platforms. The following sections discuss the response of both resistive and impedance based sensors in detail.

4.2 Resistive Gas Sensors

4.2.1 Results with various gases and organic solvents

Initial experiments were performed at room temperature to measure the response of arc produced carbon nanotubes to several analytes. However, as almost no response was observed for measurements at room temperature, an operating temperature of 200^{o}C was chosen for all further measurements. A voltage bias of 2V was chosen to maximize the signal to noise ratio as discussed.

As mentioned before, N_2 was used as the carrier gas for both gases and organic solvents. However, the concentration for each organic solvent varied as a function of their vapor pressure. The difference in concentration of the different analytes for the same flow is because of the difference in vapor pressure at a given temperature and pressure. The concentration of DMA was the lowest owing to the low vapor pressure whereas CH_3OH had the highest concentration for the same flow of N_2 through the system. Also lowering the temperature of the bubbler circuit by using an ice bath would reduce the

vapor pressure of the solvent further down. This would be good for measuring the concentration of some solvents in parts per billion (PPB) range. The sensitivity results for these analytes with the arc-produced CNTs are as shown in the following figures.

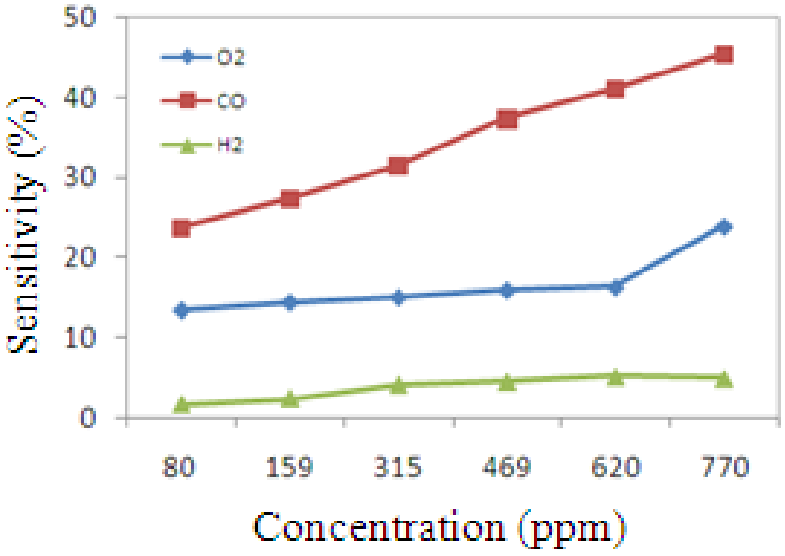

Fig 48: Sensitivity of arc produced tubes to various gaseous analytes

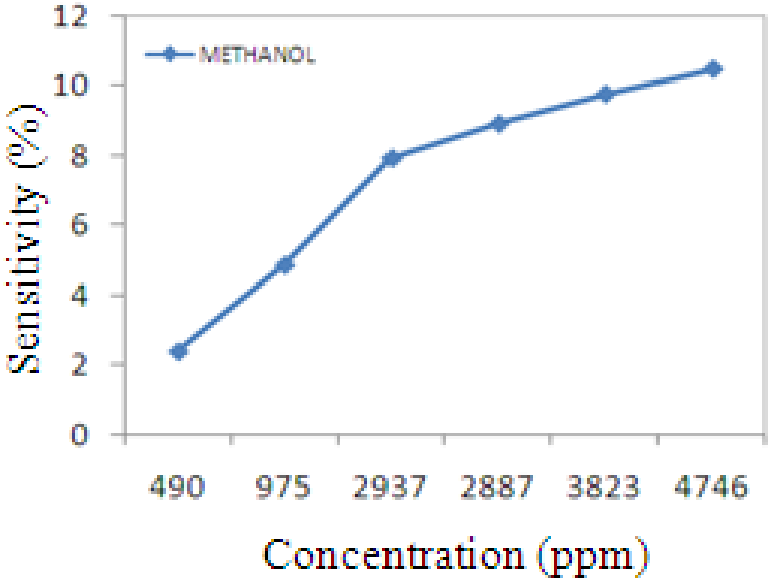

Fig 49: Sensitivity of arc produced tubes to CH_3OH

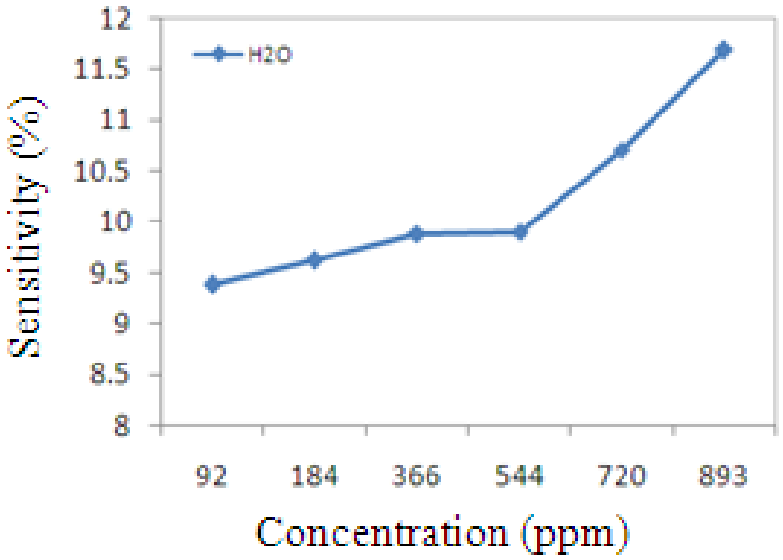

Fig 50: Sensitivity of arc produced tubes to H_2O

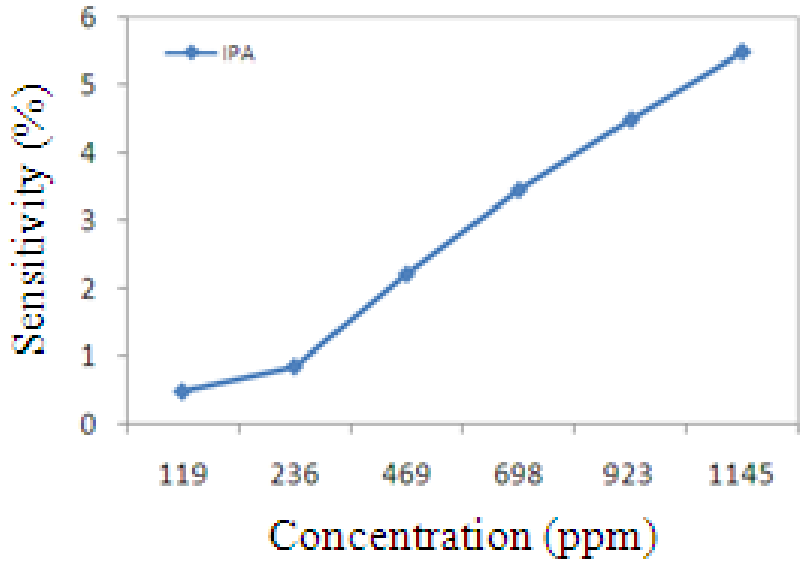

Fig 51: Sensitivity of arc produced tubes to IPA

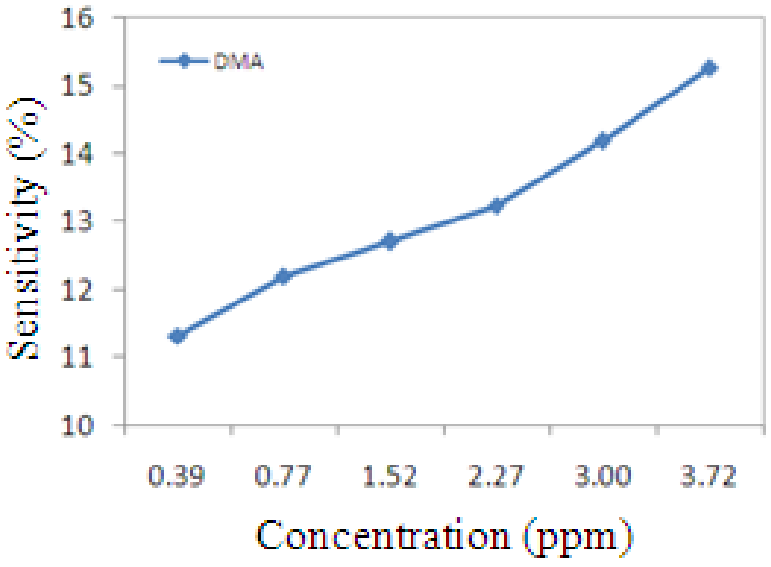

Fig 52: Sensitivity of arc produced tubes to Di-Methyl Amine

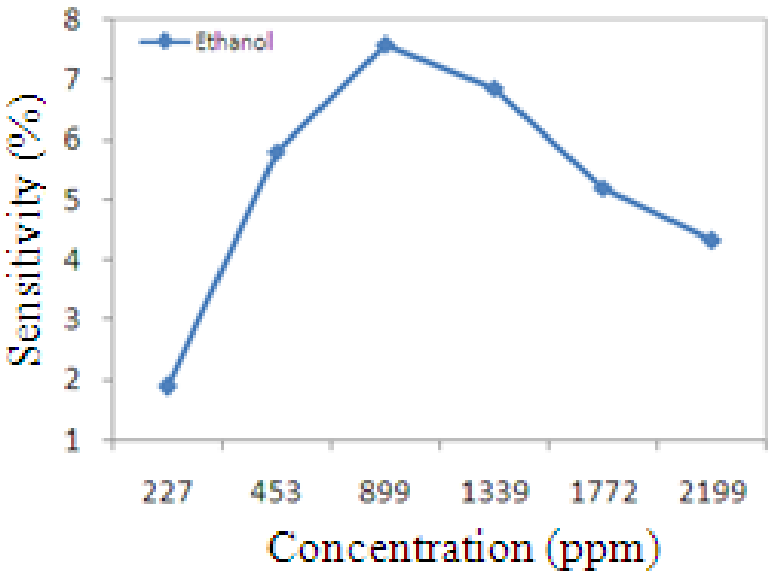

Fig 53: Sensitivity of arc produced tubes to C_2H_5OH

Sensitivity of the CNTs to different analytes for different gas flows is shown above. The response to CO was the maximum when compared to O_2 and H_2 at the given operating conditions. Sensitivity on the order of 24% was observed at 80 PPM CO as compared to values of sensitivity about 15% for O_2 and 3% for H_2. However the sensitivity to different solvents cannot be directly compared using the above data as all the solvents do not have the same concentrations owing to different vapor pressures at room temperature. However this can either be done by varying the temperature in order to measure the sensitivity of the tubes to these analytes at a constant value of concentration or comparing sensitivities at some specific concentration common to all or most of the solvents. This can be seen in Table 11 where the sensitivity of the CNTs is compared to the approximately equal concentrations of the solvents.

Solvent	Concentration (PPM)	Sensitivity %
IPA	468	2.2
C_2H_5OH	453	5.8
CH_3OH	490	2.4
H_2O	544	8.9

Table 11. Comparison of sensitivity of arc CNTs to different solvents.

As evident the response of the tubes is approximately the same for IPA and Methanol as a given concentration and operating temperature but the response to Ethanol is greater for the same range of concentration. Also the data suggests that the tubes show better sensitivity towards H_2O which is in agreement with the literature wherein humid air is used as a recovery gas for oxidizing gases. Values of sensitivity of about 15 % were

observed for as low as 3.72 PPM of DMA. With further optimization in gas sensor fabrication techniques, response to DMA in the PPB range can be expected.

4.2.2 Comparison with ZnO Based Gas Sensors

Sensitivity values for both ZnO and arc produced CNTs were recorded for the same gases and organic solvents. The sensitivity values of both the sensing materials to these analytes were compared. This comparison can be made as the process parameters - operating temperature and applied bias - and sensor heads used – MSP632 - for both these materials were identical. Fig 54 plots the sensitivity towards CO and O_2 versus concentration for both these sensing materials.

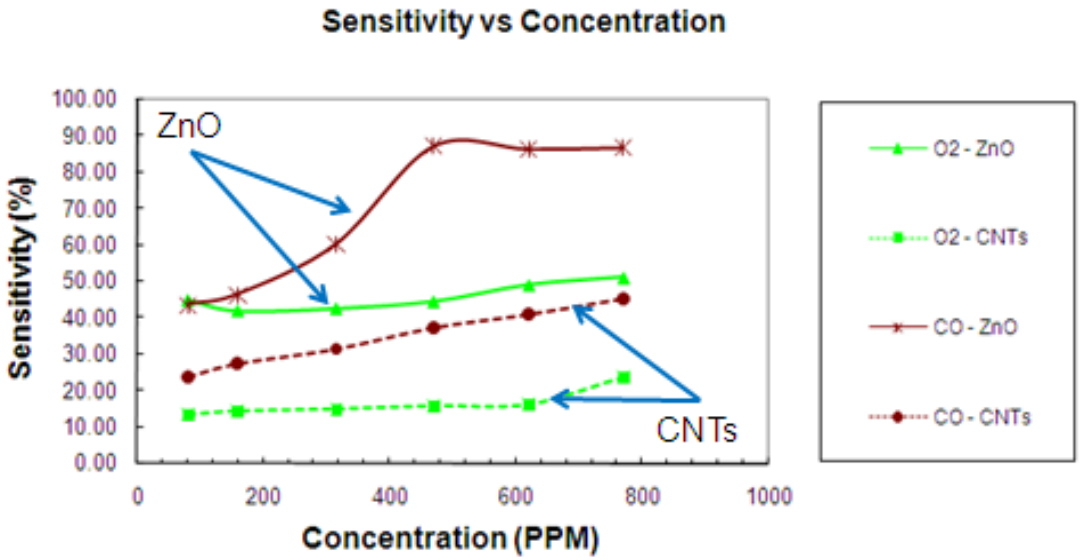

Fig 54: Sensitivity vs PPM for both ZnO nano-platelets and Arc Produced CNTs.

Better values were observed with ZnO nanoplatelets when compared to arc tubes for all the analytes. This was probably because of the extremely low amount of

CNTs used for the gas sensor fabrication which limits the surface area thus impacting the sensitivity results to different analytes. Even better results were anticipated by the use of HiPCo produced SWCNTs as they are better quality tubes as compared to the arc produced tubes. Sensing results with HiPCo tubes are discussed in the following section.

4.3 Impedance Spectroscopy Measurements

As discussed in the previous sections, high operating temperatures were used in order to record sensitivity of arc produced CNTs to various analytes. These high temperatures limit the integration of the sensors in micro-machined devices. Also, to ensure that the inter-digitated electrodes were not shorted with the arc produced CNTs, only a small amount of material was used for the fabrication of the gas sensors. This potentially reduces the surface area for gas sensing thus resulting in lower sensitivity values. In order to overcome these issues, MEMS based sensors were used with HiPCo produced tubes. The cross-section of this sensor fabricated using HiPCo tubes is shows in Fig 14.

The resistance of the SWCNT network using the MEMS based sensors was measured under various analytes and concentrations. The sensor did not show any resistive response to the analytes at room temperature with a DC bias of 2.5V applied across the electrodes. This was because of the high conductive nature of the HiPCo SWCNTs. As discussed in previous chapters, SWCNTs can be semiconducting in nature depending on chirality. This semiconducting behavior of the SWCNT network induces a capacitive component [56,57] on being exposed to certain analytes. In order to record this response of HiPCo produced SWCNTs; impedance spectroscopy was implemented

to analyze the sensor's response. Sensitivity values were recorded with an AC bias of 2.5V across the electrodes over a frequency range of 1 kHz to 1 MHz in a N_2 ambient pressure at room temperature. Higher response, when compared to DC measurements, was observed for the sample with impedance spectroscopy.

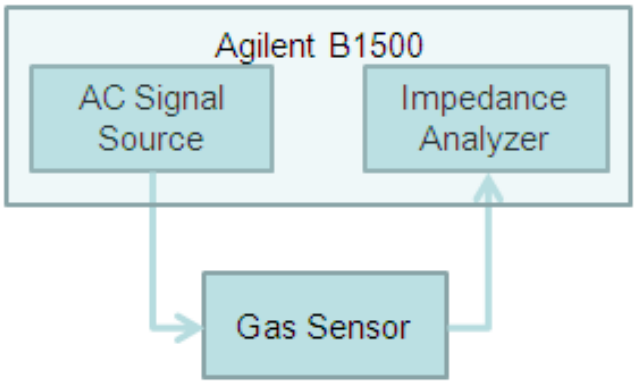

Fig 55: Circuit model for the impedance based measurements

Circuit model used for the impedance spectroscopy measurements is shown in Fig 55. The AC signal source was used to bias the electrodes of the sensor and the impedance of the cell was measured using the impedance analyzer of the Agilent B1500 parametric analyzer. The equivalent circuit of the model can be best described by Randles cell as in Fig 56.

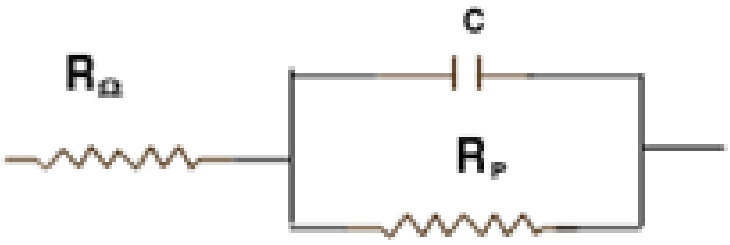

Fig 56: Showing Randles cell as the equivalent circuit for the impedance model used.

The cell connects a capacitor (double layer capacitance) and resistor Rp (polarization resistance) in parallel to an un-compensated series resistance given by R_Ω. The impedance of Randles cell; when calculated can be given by Eq 13.

$$R_\Omega + \frac{R_p}{1 + (\omega R_p C)^2} + j\left(\frac{-(\omega R_p^2 C)}{1 + (\omega R_p C)^2}\right) \qquad \text{Eq 13.}$$

As evident from Eq 13, at lower frequencies the imaginary part of the impedance equals zero. Thus the equivalent impedance of the sensor equals to R_Ω + Rp at zero frequency. Similarly, when the frequency value approaches infinity the impedance of the sensor is given by R_Ω. Fig 57 shows the functional form of Randles cell when real part of impedance is plotted against imaginary part.

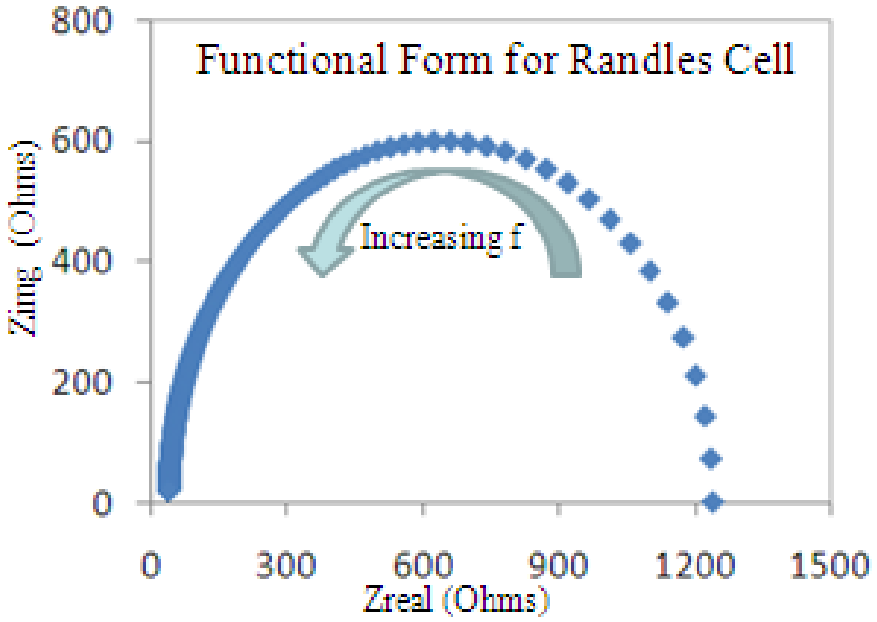

Fig 57: Showing functional form of Randles cell.

Fig. 58 illustrates a typical Nyquist plot depicting the real part of the SWCNT sensor impedance versus the imaginary part. As stated above, the frequency was varied from 1 kHz to 1 MHz with an AC bias of 2.5V in N_2 ambient. As mentioned before, at lower frequencies the capacitive component of the SWCNTs is negligible; hence any change in the impedance of the sample at lower frequencies is associated to the resistance of the sample. Hence the value of the impedance at 1 KHz frequency was given by the sum of R_Ω and Rp. The sensitivity of the sensor S was thus calculated as in Eq (1) [18, 51] where R_{air} is the resistance of the sample in N_2 ambient and R_{gas} is the resistance observed after a 5 Min exposure to the analyte. Other researchers [56] have also reported sensitivity results based on capacitance (extracted from the impedance equation mentioned above). The change in capacitance of the sensing film on reaction with the analyte can be used to extract other important parameters such as relaxation times for the sensor. However it was not in the scope of this project.

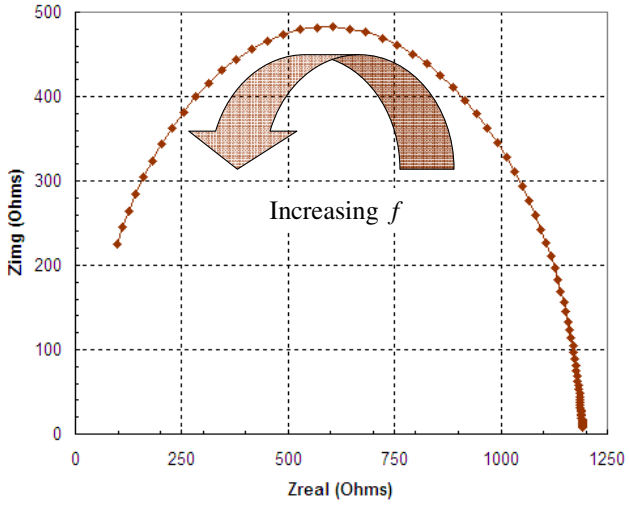

Fig 58: Nyquist plot for SWCNT network at room temperature.

Chapter II mentions the experimental details for recording the sensitivity of the HiPCo based SWCNT network. The twofold approach adopted in order to understand the gas sensing response of the SWCNT network to different analytes involved, varying exposure time and varying the concentration of the analytes in two different sets of experiments. These approaches are discussed in two different sections below.

4.3.1 Results for varying exposure time

Sensitivity of SWCNT network was measured for NH_3, IPA, CO, CH_3OH, C_2H_5OH and DMA. The response of the sample to NH_3 for varying exposure time can be seen in Fig 59 as follows.

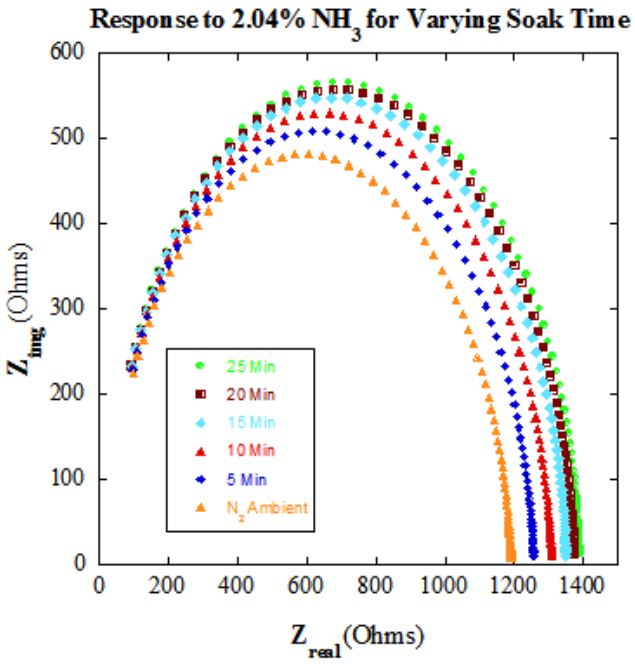

Fig 59: Nyquist plots obtained for SWCNT network for Varying Exposure Time (NH_3).

The SWCNT network showed 15.27% sensitivity on exposure to 2% NH_3 at room temperature. This was a significant increase compared to other reports of NH_3 sensitivity [58] (~22.5% with multi-walled carbon nanotubes on exposure to 20% NH_3 at room temperature). Values of sensitivity on the order of 7.66% and 10.45% were recorded for concentrations as low as 850 and 950 PPM respectively. The sensitivity of the SWCNT network was also recorded for increasing exposure times at a fixed concentration for different analytes as tabulated in Table 12. Fig 60 plots the sensitivity versus exposure time for these analytes.

Exposure Time (min)	Ethanol		DMA		Methanol		CO		IPA		NH3	
	Conc (%)	Sensitivity	Conc (%)	Sensitivity	Conc (%)	Sensitivity	Conc (%)	Sensitivity	Conc (%)	Sensitivity	Conc (%)	Sensitivity
5	6.05	0.42	0.01	0.70	14	2.00	2.04	2.77	4.02	3.23	2.04	5.01
10	6.05	1.44	0.01	1.45	14	3.98	2.04	4.81	4.02	6.90	2.04	9.87
15	6.05	2.52	0.01	2.65	14	5.18	2.04	6.35	4.02	8.86	2.04	13.32
20	6.05	3.50	0.01	3.98	14	5.97	2.04	7.30	4.02	10.20	2.04	15.35
25	6.05	4.28	0.01	6.16	14	6.96	2.04	7.97	4.02	10.98	2.04	16.74

Table 12: Sensitivity values for different analytes with varying exposure time (min).

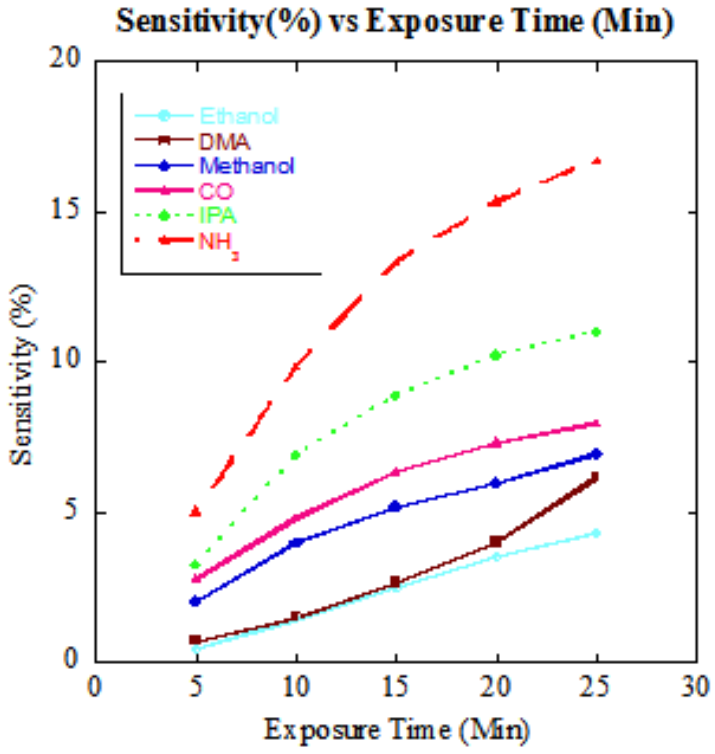

Fig 60: Sensitivity values for varying exposure times (min).

Data suggests saturation of the SWCNT network for increasing exposure times at high concentrations of analytes. The sensor showed ~6% sensitivity to 0.01% (100 PPM) DMA for an exposure time of 25 minutes. Whereas, sensitivity values recorded for other solvents were 16.74%, 10.98%, 7.97%, 6.96% and 4.28% for concentration levels of 2.04%, 4.02%, 2.04%, 14% and 6.05% of NH_3, IPA, CO, CH_3OH and C_2H_5OH respectively. Saturation of the SWCNT network was observed at higher levels of concentration is in accordance with the hypothesis of occupation of preferred sites as discussed in the preceding sections. However the observed saturation times varied for different analytes. Fig 50 suggests saturation time of about 15 min for NH_3 when compared to 10 min for IPA. The sensor shows an exceptional response to DMA when compared to the other analytes. Sensitivity values of about 16% were recorded for saturation of the SWCNTs to NH_3 with both the approaches.

4.3.2 Results for varying analyte concentration

The second set of experiments involved recording the sensitivity of the SWCNT network for various concentration values of different analytes. The response of the sample to NH_3 for varying exposure time can be seen in Fig 61 as follows.

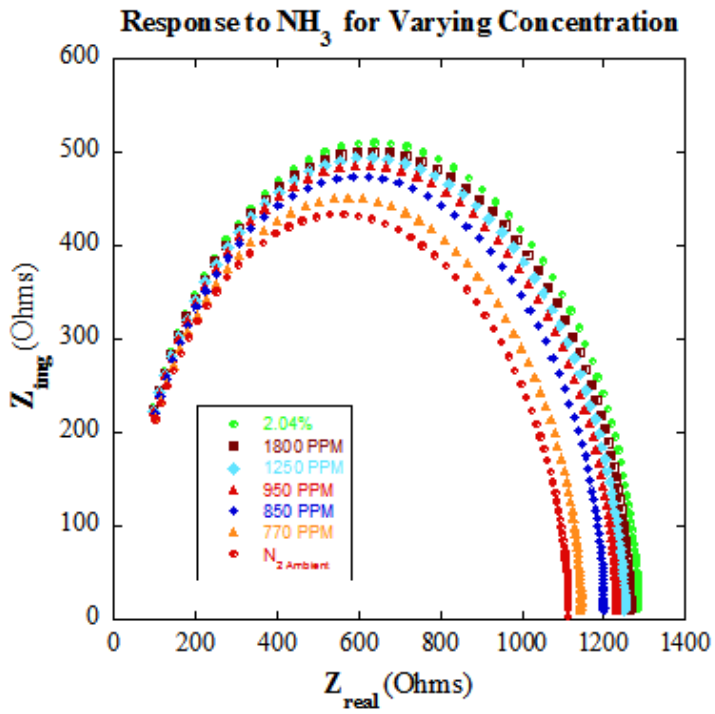

Fig 61: Nyquist plots obtained for SWCNT network for varying concentration (NH_3).

Table 15 shows values of concentration and sensitivity for different analytes and different gas flows. The tabulated values were recorded to observe the lowest concentration of the analyte that could be detected with the SWCNT network. Fig. 62 plots sensitivity values tabulated in Table 13 for each analyte.

Conc ID	Ethanol		CO		IPA		Methanol		NH3	
	Conc (%)	Sensitivity	Conc (%)	Sensitivity	Conc (%)	Sensitivity	Conc (%)	Sensitivity	Conc (%)	Sensitivity
1	0.42	0.10	0.077	1.44	0.29	2.64	0.92	2.36	0.077	2.56
2	0.52	0.12	0.095	2.83	0.35	3.12	1.13	3.12	0.095	10.45
3	0.68	0.20	0.125	3.30	0.46	3.55	1.47	3.78	0.125	12.07
4	0.96	0.60	0.180	3.82	0.65	4.12	2.09	4.64	0.180	13.42
5	6.05	0.92	2.040	4.35	4.02	4.95	14.01	6.59	2.040	15.27

Table 13: Sensitivity values for various analytes for the varying concentration study

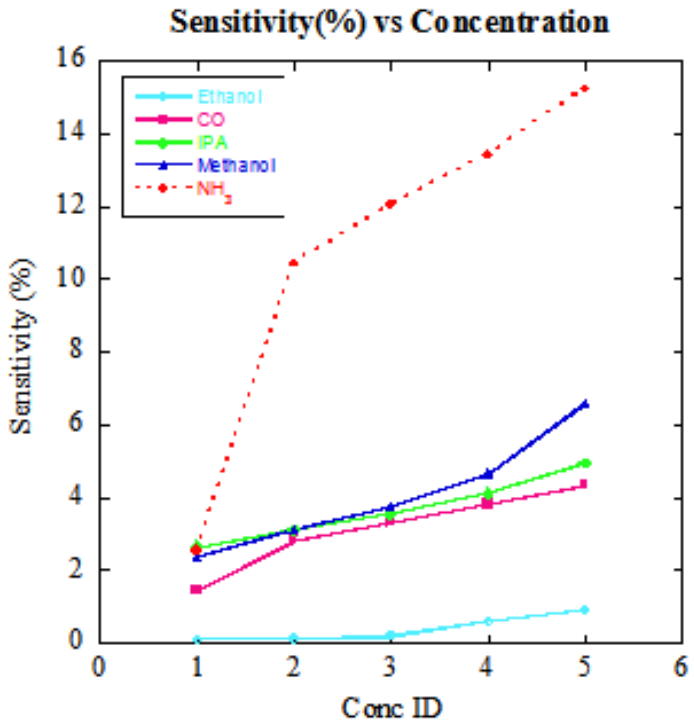

Fig 62: Sensitivity values for varying concentrations.

Better response for both the analytes in gaseous form (NH_3 and CO) with values of sensitivity on the order of 15.27% and 3.82% were recorded for as low as 0.18% analyte. These values were higher than those recorded for the solvents which were 2.64%, 2.36% and 0.10% for concentration levels of 0.29% , 0.92% and 0.42% of IPA, CH_3OH and C_2H_5OH respectively. The low sensitivity towards organic solvents is believed to be because of the bulkier nature of molecules which limits chemisorption only to the surface of the SWCNT network. High response of about 15% was observed for as low as 2% NH_3 whereas sensitivity on the order of 0.92% was recorded for about 6.05% C_2H_5OH. Lower increase in sensitivity or saturation was observed for further increase in the concentration of the analytes, because of the occupation of the preferred reaction sites thus inhibiting any further charge transfer to the sensing material.

The sensing mechanism was believed to be chemisorption of the analyte to surface of SWCNTs, as the sensor showed no recovery on flooding the chamber with industrial grade air. The sensor was however recovered in room ambient over a period of 4 to 6 hours depending on the chemisorbed analyte. Data suggests saturation in sensitivity on long exposure times to the analyte which is because of occupancy of all preferred sites in the material [59].

Results obtained with HiPCo produced SWCNT network at room temperature were comparable to the values of sensitivity shown by other researchers [42]. However, when compared to the other sensing materials used for the project, ZnO based sensors show the maximum sensitivity to different analytes at an operating temperature of 200^{o}C. The choice as to which material can be used for commercial sensors fabrication needs to be made requirements of the customer i.e. ZnO would be the preferred choice of sensing material where high sensitivity is required but operating temperature may not be a concern and HiPCo based sensors can be used where the sensitivity requirement is not very high but the operating temperature is a more critical requirement.

CHAPTER V

CONCLUSION AND FUTURE WORK

5.1 Research Summary

ZnO nano-structures and SWCNTs have been tested as chemical sensors. Resistive measurements and impedance spectroscopy were both successfully implemented to fabricate gas sensors for various gases and organic solvents. Also, in-depth study was successfully conducted to understand the effect of different device parameters – inter electrode spacing and number of electrodes - and process parameters – temperature, applied bias and analyte concentration - on gas sensitivity. Other experiments also demonstrated the effect of other factors such as carrier gas flow, surface area, porosity and catalysts on gas sensitivity.

Gas sensitivity was found to depend on the porosity and surface area of the ZnO nano-structures. Presence of a catalyst significantly enhances the gas sensitivity and lowers the operating temperatures. Incomplete recovery of the ZnO sensors at room temperature was attributed to the formation of water at the surface. Saturation of the ZnO sensors was observed at higher concentrations owing to the short exposure time to the analyte. Sensitivity did not vary significantly with carrier gas flows, however faster response and quick recovery was observed for higher carrier gas flows. High sensitivity of the ZnO sensor at low temperatures is attributed to both the increased surface area and the porosity of the nano-structures. Values in excess 80% of ZnO nanostructures for H_2 gas were observed at room temperature. Measurements at higher temperature (150^oC)

show even higher sensitivities, near 96% for a 20 PPM concentration of H_2. Results of ZnO based nano-materials were also successfully recorded for different gases. Values of sensitivity on the order of 60% were observed at 315 PPM CO as compared to values of sensitivity about 42% for O_2 and 29% for NH_3 at similar values of concentration at an operating temperature of 200^oC. Results for organic solvents like C_2H_5OH, CH_3OH and H_2O were also recorded with sensitivity values of 77.76%, 70.26% and 38.43% respectively for concentration values approximating 500 PPM.

Designed experiments were conducted to understand effects of various device and process parameters. For varying spacing study, negative dependence on sensitivity was seen with spacing between the electrodes with lower sensitivity values being observed for higher spacing. Maximum effect of bias was observed for lower concentration values and this difference in sensitivity was observed to reduce with increasing spacing. Lower sensitivity values of values of about 60% for 60PPM H_2 gas were recorded as compared to that of 81.7% for MSP-632 for the same concentration of the analyte due to the difference in device parameters.

The sensitivity of the sensor was recorded to increase with the increase in the number of electrodes. Applied voltage bias was not identified as a significant factor for gas sensitivity with constant spacing between the IDEs. Saturation of the sensitivity was observed for higher values of concentration. Higher sensitivity values nearing 70% were achieved with 30 IDEs for 60 PPM H_2 when compared to 60% for 60 PPM of H_2 with 20 IDEs. Gas sensitivity was impacted more at higher concentration for less number of IDEs due to the limited number reaction sites.

Interaction effects were observed and implemented to understand and model the behavior of the gas sensor. Though the obtained results were highly dependent on the range of operation chosen for the process parameters, they were representative of previously observed results with the nano-platelets.

Sensitivity of arc produced SWCNTs was measured to various gases and organic solvents. Values on the order of 24% were observed at 80 PPM CO as compared to values of sensitivity about 15% for O_2 and 3% for H_2. Sensitivity values for the organic solvents were compared at some specific concentration common to all or most of the solvents. Higher sensitivity towards H_2O – 8.9% for 544 PPM – was observed when compared to values like 2.2%, 2.4% and 5.8% for 468 PPM, 490 PPM and 453 PPM of IPA, CH_3OH and C_2H_5OH respectively. Also, sensitivity of 15% was measured for as low as 4 PPM of DMA which suggests the capability of PPB levels of DMA using SWCNTs.

Lower values of sensitivity were observed for the arc produced CNTs when compared to the ZnO nano-platelets owing to the small amount of material used for gas sensor fabrication.

Sensitivity to different analytes was measured using impedance spectroscopy for HiPCo produced SWCNT network. Higher response, when compared to DC measurements, was observed for the sample with impedance spectroscopy. The results were successfully recorded for different gases and organic solvents, by varying exposure time while maintaining the concentration of the analyte as a constant. Sensitivity values nearing 6% for 0.01% (100 PPM) DMA for an exposure time of 25 minutes. Results for sensitivity recorded for other solvents were 16.74%, 10.98%, 7.97%, 6.96% and 4.28%

for concentration levels of 2.04%, 4.02%, 2.04%, 14% and 6.05% of NH_3, IPA, CO, CH_3OH and C_2H_5OH respectively. Saturation of the SWCNT network was observed at higher levels of concentration, with the observed saturation times varying for different analytes. Exceptional response to DMA was observed when compared to the other analytes.

Sensitivity was also recorded for various concentration values of different analytes. Higher response was observed for gaseous analytes. Results on the order of 15.27% and 3.82% were recorded for as low as 0.18% of both NH_3 and CO. For the organic solvents, values approximating 2.64%, 2.36% and 0.10% for concentration levels of 0.29%, 0.92% and 0.42% of IPA, CH_3OH and C_2H_5OH respectively. The low sensitivity towards organic solvents was believed to be because of the bulkier nature of molecules. Results obtained with HiPCo produced SWCNT network at room temperature were comparable to the values of sensitivity shown by other researchers.

5.2 Future Work

The sensitivity of the gas sensor was successfully modeled for different device and process parameters; however, one of the major factors i.e. the material properties (morphology, porosity and surface area) was not varied for modeling the response of the sensor. Our future works entails correlating the sensitivity of the gas sensors to the material properties in addition to the device and the process parameters. Further work is also required to develop standard methods for fabricating gas sensors. This could help

minimize the variation in gas sensitivity due to the variation in porosity and surface area of the sensing film.

Also, further advancements to the gas sensor performance would be to improve the selectivity of the sensor thus enabling detection of one gas in a mix gas environment. This can be achieved by using different catalysts like Cu to enhance detection of CO and Pt for enhancing sensitivity to H_2 gas respectively. These catalysts can either be incorporated in the sensor as the metal for the inter-digitated electrodes or by decorating the sensing film with metal nano-particles. However, the response of the sensor to these specific gases needs to be calibrated in a mix gas environment for the relative sensitivity needs to be monitored to ensure detection. This concept was successfully implemented in this work to detect different gases and organic solvents with arc produced CNTs.

As was seen in this thesis, different types of fabricating techniques were used to fabricate gas sensors with different types of carbon nano-tubes. However, the amount of the material used for the fabrication process was very small, owing to the high conductive nature of the material. One of these techniques was tried in this work but not fully explored. This was, using as-grown multiwalled carbon-nanotubes MWCNTs for gas sensor fabrication. MWCNTs have been reported to detect different analytes by various researchers. The in-house capability to grow MWCNTs on silicon di-oxide attracts interest to implement this technique for sensor fabrication. The advantages of using this technique will be controlled fabrication and high surface area for gas sensitivity as the MWCNTs grown on SiO_2 results in horse hair like grown films.

In addition to developing standard fabrication techniques with carbon nano-tubes, various methods can be implemented in order to improve the selectivity of these tubes

for different gases and organic solvents. This can be achieved by decorating carbon nano-tubes with metal nano-particles which act as catalysts for improved response or by filling the carbon nano-tubes with these metal nano-particles using capillary action. Other methods include decorating CNTs with groups of organic molecules. The advantage of using organic molecules over metal nano-particles is that these molecules can be tailored to enhance sensitivity to different analytes depending on the affinity of various organic groups to various analytes. Further investigation is also required to correlate the sensitivity of different types of tubes like HiPCo produced SWCNTs, in-house produced Laser ablated SWCNTs and MWCNTs to their material properties. This involves extensive research like determining dimensional properties, purity assessment and characterization of electrical behavior of different tubes.

APPENDIX

As for the single level sensors P-type [100] 4" silicon wafers were used as starting substrates. The backside of the wafers was polished using a Strausbaugh Chemical Mechanical Planarization tool with 8 PSI pressure on the polish pad.

As discussed previously, diaphragms were needed to optimize the heat uniformity across the sensor pad. In order to accomplish this, 1500Å of silicon nitride was deposited over a 500Å pad oxide to relieve stress. Backside photolithography (coat, expose and develop) was then performed using the Karl Suss Mask Aligner (MA-150) to pattern the diaphragms. Nitride and oxide layers were patterned and etched from the backside to allow etching of Silicon for the formation of the diaphragms in KOH over a period of 8 hours. Silicon nitride on the front side was used as a mask to protect the wafer in KOH.

An oxide layer - 5000 A thick- was then grown - - to isolate the first level metal from the substrate after the wafers were processed through a de-contamination clean. Following the oxide growth, Lift-off Resist LOR-5A was spin coated on the substrates for Pt/Cu lift-off. The heaters were aligned to the diaphragms using a in-house devised method. Proper backside alignment is necessary to avoid any heat loss to the substrate. Fig 63 describes the backside alignment technique.

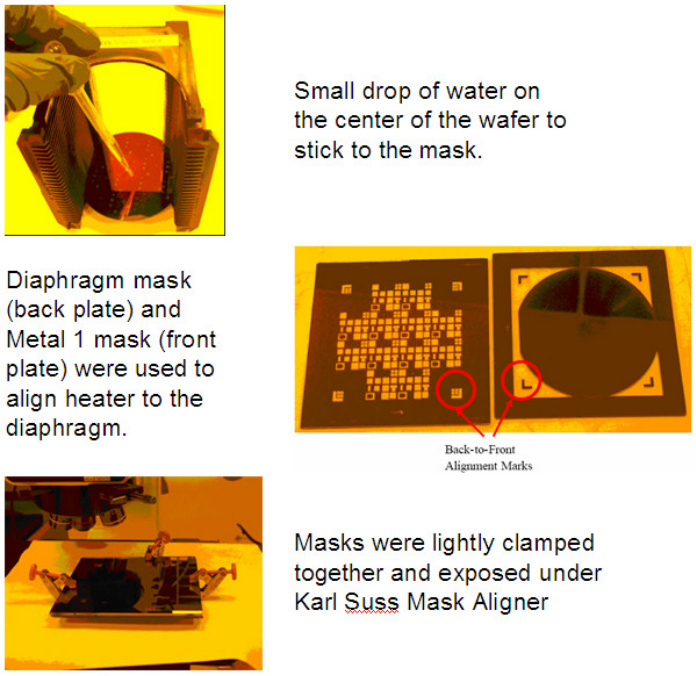

Fig 63: Process Steps for backside alignment technique.

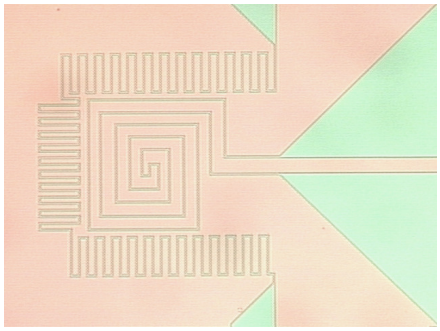

Fig 64: Top-Down Image of the heater and temperature Sensor (Ti/Pt Stack)

As stated before, a Ti/Pt stack was used to ensure adhesion to the underlying oxide. However, this causes adhesion failures of the ILD – overlaying oxide - to the Platinum underneath. A Ti/Pt/Ti stack for the heater and the temperature sensor would allow adhesion to both the underlying and overlaying oxide layers. Fig 64 shows a top-down image of the sensor with the first level metal - heater and temperature sensor - defined.

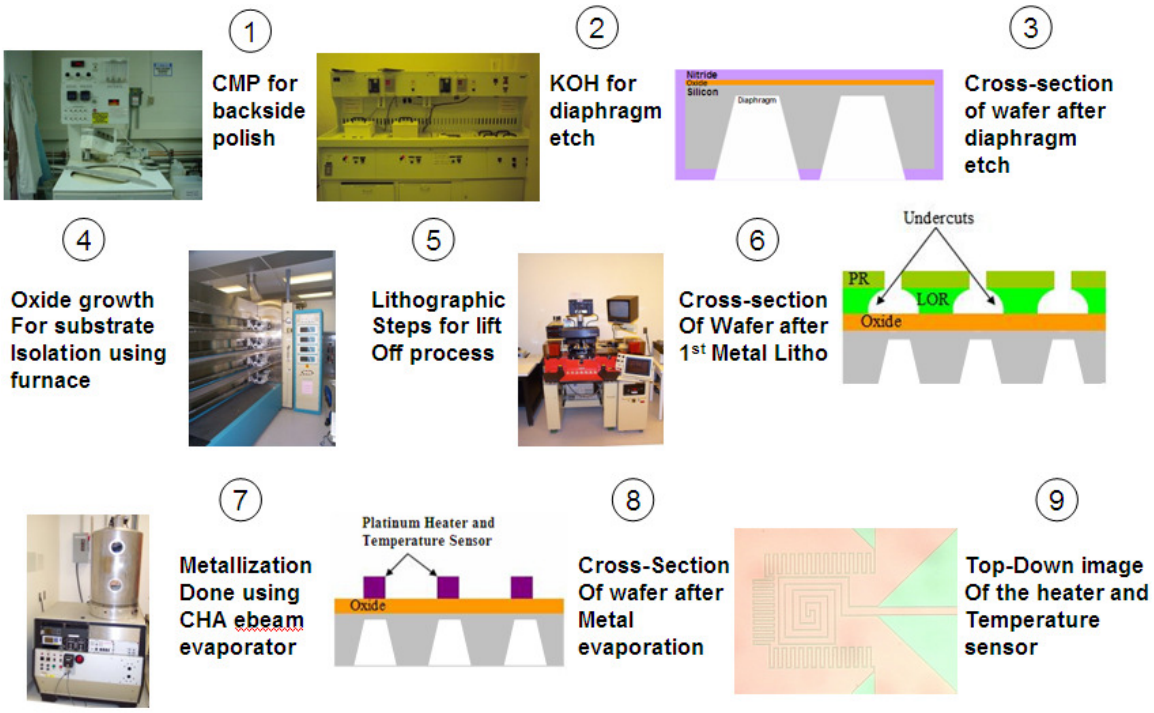

Fig 65: Flow for the dual level MEMS based gas sensor.

The diagrammatic representation of the dual level sensors is as shown in Fig 65. However, the sensor was not fully fabricated due to the adhesion issues of the overlying oxide to the heater and temperature sensor. Considering financial and time constraints, dual level gas sensors were not re-fabricated and the commercial sensor heads were used for all high temperature measurements.

Process Flow for fabrication of dual level MEMS Sensor Platforms.

1. Obtain qty 12, 4” n-type wafers
2. CMP back side
3. CMP Clean
4. RCA Clean
5. Grow 500 Å pad oxide , Recipe 250
6. Deposit 1500 Å Nitride (deposited on the front and back side)
7. Spin coat Resist on back side of wafer
8. Expose and Develop the diaphragms
9. Spin coat Resist on front side of wafer (to prevent oxynitride etch)
10. Etch oxynitride (from backside), 1 min. dip in BOE, Rinse, SRD
11. Plasma Etch Nitride on back of wafer, Lam-490
12. Wet etch of pad oxide, Rinse, SRD
13. Strip Resist both sides
14. Etch Diaphragm in KOH, ~8 hours
15. Decontamination Clean
16. RCA Clean
17. Hot Phosphoric Acid Etch of Nitride
18. BOE etch of pad oxide
19. Grow 5000Å oxide
20. Put Down LOR.
21. Spin Coat 1813 Resist.
22. Expose and Develop , For heater Pt (use lift off method)
23. Develop 1813 and LOR to form undercuts.
24. Evaporate Platinum for the heater using e-beam evaporator.
25. Lift Off resist
26. RCA Clean
27. Evaporate 1µm SiO2
28. Spin Coat resist
29. Expose and Develop Vias
30. Etch in BOE, Rinse, SRD
31. Strip Resist
32. RCA Clean, include extra HF
33. Put Down LOR.
34. Spin Coat 1813 Resist.
35. Develop 1813 and LOR to form undercuts.
36. Evaporate Platinum for the ID fingers using e-beam evaporator.
37. Lift-off Resist

REFERENCES

[1] Y. Lv, L.Guo, H. Xu and X. Chu. Gas-sensing properties of well-crystalline ZnO nanorods grown by a simple route.

[2] S. Basu and A. Dutta, Mater. Room-Temperature hydrogen sensors based on ZnO.

[3] G. Rao and D. Rao, Gas sensitivity of ZnO based thick film sensor to NH_3 at room temperature.

[4] J.B. Baxter, E.S. Aydil, Dye-sensitized solar cells based on semiconductor morphologies with ZnO nanowires.

[5] D.C. Altamirano-Jua´rez, G. Torres-Delgado, S. Jime´nez-Sandoval, O. Jime´nez-Sandoval, R. Castanedo-Pe´rez, Sol. Energy Mater. Sol. Cells 82 (2004) 35.

[6] E.J. Ibanga, C. Le Luyer, J. Mugnier, Mater, Chem. Phys. 80 (2003) 490.

[7] W.T. Chiou, W.Y. Wu, J.M. Ting, Diamond Relat. Mater. 12 (2003) 1841.

[8] Anna.Og. Dikovska, P.A. Atanasov, A.Ts. Andreev and B.S. Zafirova, ZnO thin film on side polished optical fiber for gas sensing applications.

[9] P. Bhattacharyya, P.K. Basu, H. Saha, S. Basu, Fast response methane sensor using nanocrystalline zinc oxide thin films.

[10] S. Kar, B.N. Pal, S. Chaudhuri, and D. Chakravorty, One-Dimensional ZnO Nanostructure Arrays: Synthesis and Characterization.

[11] S. Kar, B.N. Pal, S. Chaudhuri and D. Chakravorty, J. Phys. Chem. B 2006, 110, 4605-4611.

[12] J.J. Delaunay, N. Kakoiyama and I. Yamada, Materials Chemistry and Physics 104 (2007) 141–145.

[13] P.Hari, M.Baurner. W.D.Tennyson and L.A.Bumm, ZnO nanorod growth by chemical bath method.

[14] A.Aroraa, A.Aroraa, V.K.Dwivedia, P.J.Georgeb, K.Sreenivasc and V.Gupta, Zinc oxide thin film-based MEMS acoustic sensor with tunnel for pressure compensation

[15] A. Maiti, J. Hoekstra, J. Andzelm, N. Govind, A. Ricca, A. Svizhenko, H. Mehrez and M. P. Anantram. Electronic transport through carbon nanotubes – effect of contacts, topological defects, dopants and chemisorbed impurities.

[16] J. Li, Y. Lu, Q. Ye, M. Cinke, J. Han, and M. Meyyappan, Carbon Nanotube Sensors for Gas and Organic Vapor Detection.

[17] http://nanopedia.case.edu/NWPage.php?page=nanotube.chirality

[18] Y.M. Wong, W.P. Kang, J.L. Davidson, A. Wisitsora-at, K.L. Soh. A novel microelectronic gas sensor utilizing carbon nanotubes for hydrogen gas detection.

[19] G. Sberveglieri, Gas Sensors – Principles, Operation and Developments

[20] A.Saluja, J.Pan, L.Kerr, E.Cho and S.Hubbard, Gas Sensing Properties of Porous ZnO Nano-Platelet Films.

[21] C. Zamani, K.Shimanoe, N.Yamazoe, Capacitive-type gas sensors combining silicon semiconductor and NaNO2-based solid electrolyte for NO2 detection.

[22] H. Steffes, A. Schleunitz, U. Gernert, R. Chabicovsky, E. Obermeier, A novel optical gas sensor based on sputtered InxOyNz films with gold-nano-dots.

[23] T. Yamaguchi, T. Kiwa, K. Tsukada, K. Yokosawa, Oxygen interference mechanism of platinum–FET hydrogen gas sensor.

[24] L. Czepirski, M.R. Balys, E. K. Czepriska, Some generalization of Langmuir adsorbtion isotherm.

[25] H.S Fogler & M.N Grumen. Elements of Chemical Reaction Engineering.

[26] S. Roy and S. Basu, Improved zinc oxide film for gas sensor applications**.**

[27]T. Hsueh, Y. Chenb, S. Changa, S. Wang, ZnO nanowire-based CO sensors prepared on patterned ZnO:Ga/SiO2/Si templates.

[28] G. Lu, N. Miura, N. Yamazoe, High-temperature hydrogen sensor based on stabilized zirconia and a metal oxide electrode.

[29] C.M. Ghimbeu, J. Schoonman, M. Lumbreras and M. Siadat. Electrostatic spray deposited zinc oxide films for gas sensor applications.

[30] Q. Wan, Q. H. Li, Y. J. Chen, and T. H. Wanga. Fabrication and ethanol sensing characteristics of ZnO nanowire gas sensors.

[31] X.L. Cheng, H. Zhao, L.H. Huo, S. Gao, J.G. Zh, ZnO nanoparticulate thin film: preparation, characterization and gas sensing properties.

[32] Z. Sun, L. Liu, L. Zhang and D. Jia, Rapid synthesis of ZnO nano-rods by one-step, room-temperature, solid-state reaction and their gas-sensing properties

[33] J. Delaunay , N. Kakoiyama, I. Yamada, Fabrication of 3D network of ZnO tetratpods & its response to C_2H_5OH.

[34] L. Bie , X. Yan, J. Yin, Y. Duan, Z. Yuan, Nanopillar ZnO gas sensor for hydrogen and ethanol.

[35] S. Choopun, N. Hongsith, P. Mangkorntong, N. Mangkorntong, Zinc oxide nanobelts by RF sputtering for ethanol sensor.

[36] H. Xu, X. Liu, D. Cui , M. Li and M. Jiang, A novel method for improving the performance of ZnO gas sensors.

[37] H. Gonga, J.Q. Hua, J.H. Wang, C.H. Onga and F.R. Zhub Nano-crystalline Cu-doped ZnO thin film gas sensor for CO.

[38] A.Star,V.Joshi, S.Skarupo, D.Thomas, and J.Christophe P. Gabriel, Gas Sensor Array Based on Metal-Decorated Carbon Nanotubes.

[39] A. Tchernatinsky, B. Nagabhirava, S. Desai, G. Sumanasekera, B. Alphenaar, Adsorption of Oxygen Molecules on Individual Carbon Single-walled Nanotubes.

[40] J. Andzelm, N. Govind, A. Maiti, Nanotube-based gas sensors -role of structural defects.

[41] J. Kong, M. G. Chapline, and H. Dai, Functionalized Carbon Nanotubes for Molecular Hydrogen Sensors.

[42] O.K Varghese, P.D Kichambre, D.Gong, K.G. Ong, E.C Dickey, C.A Grimes, Gas sensing characteristics of multi-wall carbon nanotubes.

[43] J. Li, Y. Lu, Q. Ye, M. Cinke, J. Han, and M. Meyyappan, Carbon Nanotube Sensors for Gas and Organic Vapor Detection.

[44] T.Zhang, M.B.Nix, B.Yoo, A. Deshusses, N.V. Myung, Electrochemically Functionalized Single-Walled Carbon Nanotube Gas Sensor.

[45] K.Hyeok, S.Y.Jeong, H.R.Hwang, Y.H.Lee, Enhanced sensitivity of a gas sensor Incorporating Single walled Carbon nanotubes Polypyrrole nano-composites.

[46] P.Qi, O.Vermesh, M.Grecu, A.Javey, Q.Wang, and H.Dai, Toward Large Arrays of Multiplex Functionalized Carbon Nanotube Sensors for Highly Sensitive and Selective Molecular Detection.

[47] J.Kong, R.Chen, N.Franklin, H.Dai, Carbon Nanotube Chemical and Mechanical Sensors.

[48] J.Kong, N.R.Franklin, C.Zhou, M.G.Chapline, S.Peng, K.Cho, H.Dai, Nanotube Molecular Wires as Chemical Sensors.

[49] N.H.Quang, M.V.Trinh, B.Lee, J.Huh, Effect of NH3 gas on the electrical properties of SWNT bundles.

[50] P. Mitra, A.P. Chatterjee , H.S. Maiti, ZnO thin film sensor.

[51] I. Sayago, E. Terradob, E. Lafuenteb, M.C. Horrillo, W.K. Maser, A.M. Benito, R. Navarro, E.P. Urriolabeitia, M.T. Martinezb, J. Gutierreza. Hydrogen sensors based on carbon nanotubes thin films.

[52] R. Zhang, and L. L. Kerr, "Controlling of ZnO morphologies by adjusting Cd concentration via Chemical Bath Deposition.

[53] M.Wilson, K.Kannangara, G.Smith, M.Simmons and B.Raguse, Nanotechnology: Basic Science and Emerging Technologies.

[54] C.Philip, P.Avouris.Nanotubes for Electronics. Scientific American: 67, 68, and 69.

[55] M.Jeong and C.C.Byeon, Purity Measurement of Single-Walled Carbon Nanotubes By UV-Vis-NIR absorption spectroscopy and thermogravimetric analysis.

[56] O.K.Varghese, P.D.Kichambre, D.Gong, K.G.Ong, E.C.Dickey, C.A.Grimes, Gas sensing characteristics of multi-wall carbon nanotubes.

[57] J.Kong, R.Chen, N.Franklin and H. Dai, Carbon Nanotube Chemical and Mechanical Sensors.

[58] J.Suehiro, G.Zhou and M.Hara, Fabrication of a carbon nanotube-based gas sensor using dielectrophoresis and its application for ammonia detection by impedance spectroscopy.

[59] http://www.engin.umich.edu/~CRE/course/lectures/eleven/index.htm